Atmos. Chem. Phys. Discuss., 15, 22823–22887, 2015
www.atmos-chem-phys-discuss.net/15/22823/2015/
doi:10.5194/acpd-15-22823-2015

Atmospheric Chemistry and Physics Discussions

Aircraft-measured indirect cloud effects from biomass burning smoke in the Arctic and subarctic

L. M. Zamora[1,2], R. A. Kahn[1], M. J. Cubison[3], G. S. Diskin[4], J. L. Jimenez[3], Y. Kondo[5], G. M. McFarquhar[6], A. Nenes[7,8,9], K. L. Thornhill[4], A. Wisthaler[10,11], A. Zelenyuk[12], and L. D. Ziemba[4]

[1]NASA Goddard Space Flight Center, Greenbelt, MD, USA
[2]Oak Ridge Associated Universities, Oak Ridge, TN, USA
[3]CIRES and Dept. of Chemistry and Biochemistry, University of Colorado, Boulder, CO, USA
[4]NASA Langley Research Center, Hampton, VA, USA
[5]National Institute of Polar Research, Tokyo, Japan
[6]University of Illinois at Urbana-Champaign, Urbana, IL, USA
[7]Georgia Institute of Technology, Atlanta, GA, USA
[8]Foundation for Research and Technology – Hellas, Patras, Greece
[9]National Observatory of Athens, Greece
[10]Department of Chemistry, University of Oslo, Oslo, Norway
[11]Institute for Ion Physics and Applied Physics, University of Innsbruck, Innsbruck, Austria
[12]Pacific Northwest National Laboratory, Richland, WA, USA

Received: 7 August 2015 – Accepted: 14 August 2015 – Published: 26 August 2015

Correspondence to: L. M. Zamora (laurenge@gmail.com)

Published by Copernicus Publications on behalf of the European Geosciences Union.

ACPD
15, 22823–22887, 2015

Abstract

The incidence of wildfires in the Arctic and subarctic is increasing; in boreal North America, for example, the burned area is expected to increase by 200–300 % over the next 50–100 years, which previous studies suggest could have a large effect on cloud microphysics, lifetime, albedo, and precipitation. However, the interactions between smoke particles and clouds remain poorly quantified due to confounding meteorological influences and remote sensing limitations. Here, we use data from several aircraft campaigns in the Arctic and subarctic to explore cloud microphysics in liquid-phase clouds influenced by biomass burning. Median cloud droplet radii in smoky clouds were ~ 50 % smaller than in background clouds. Based on the relationship between cloud droplet number (N_{liq}) and various biomass burning tracers (BB_t) across the multi-campaign dataset, we calculated the magnitude of subarctic and Arctic smoke aerosol-cloud interactions (ACI, where $ACI = (1/3) \times d\ln(N_{liq})/d\ln(BB_t)$) to be ~ 0.12 out of a maximum possible value of 0.33 that would be obtained if all aerosols were to nucleate cloud droplets. Interestingly, in a separate subarctic case study with low liquid water content (~ 0.02 g m^{-3}) and very high aerosol concentrations (2000–3000 cm^{-3}) in the most polluted clouds, the estimated ACI value was only 0.06. In this case, competition for water vapor by the high concentration of CCN strongly limited the formation of droplets and reduced the cloud albedo effect, which highlights the importance of cloud feedbacks across scales. Using our calculated ACI values, we estimate that the smoke-driven cloud albedo effect may decrease shortwave radiative flux by 2–4 W m^{-2} or more under some low and homogeneous cloud cover conditions in the subarctic, although the changes should be smaller in high surface albedo regions of the Arctic. We lastly show evidence to suggest that numerous northern latitude background Aitken particles can interact with combustion particles, perhaps impacting their properties as cloud condensation and ice nuclei. However, the influence of background particles on smoke-driven indirect effects is currently unclear.

ACPD
15, 22823–22887, 2015

1 Introduction

The incidence of wildfires in the Arctic and subarctic is increasing dramatically (Flannigan et al., 2009; Stocks et al., 1998), and in some areas such as boreal North America, it is expected to grow by 200–300 % over the next 50–100 years (Balshi et al., 2009). Already, periods of intense wildfires can increase regional aerosol concentrations in the Arctic twofold (Warneke et al., 2010), and the impact of smoke is increasingly being recognized as a strong contributor to Arctic haze (Hegg et al., 2009, 2010; McConnell et al., 2007; Shaw, 1995; Stohl et al., 2006, 2007). Increases in biomass burning aerosols could have a large effect on cloud dynamics (Earle et al., 2011; Jouan et al., 2012; Lance et al., 2011; Lindsey and Fromm, 2008; Rosenfeld et al., 2007; Tietze et al., 2011); in turn, smoke-derived changes to cloud microphysics may result in changes to precipitation and regional heating that are strong enough to affect dwindling regional sea ice (Kay et al., 2008; Kay and Gettelman, 2009; Lubin and Vogelmann, 2006; Vavrus et al., 2010).

However, the interactions between smoke particles and Arctic clouds are poorly quantified, in part due to the confounding effects of meteorology and surface conditions (e.g., Earle et al., 2011; Jackson et al., 2012; Jouan et al., 2012), and in part due to satellite sampling constraints over the Arctic, such as caused by the presence of many low contrast regions, multi-layer clouds (Intrieri et al., 2002), and reduced sunlight. One common way in which aerosol-cloud interactions (ACI) (also called "indirect effects", IE) (Feingold et al., 2001, 2003) are quantified is by assessing how a cloud property changes relative to some aerosol tracer or, in this case, biomass burning aerosol tracer (BB_t). Following Eq. (1), ACI estimates for a given location can be derived from aircraft measurements of cloud droplet number, N_{liq}; they can also be derived from ground-based or remote sensing retrievals of changes in cloud properties such as droplet effective radius (r_e) or cloud optical depth (τ) at constant liquid water

ACPD
15, 22823–22887, 2015

path (LWP) (Feingold et al., 2001; McComiskey et al., 2009):

$$\mathrm{ACI} = \frac{1}{3}\frac{\mathrm{d}\ln N_{\mathrm{liq}}}{\mathrm{d}\ln \mathrm{BB_t}} = -\left.\frac{\partial \ln r_{\mathrm{e}}}{\partial \ln \mathrm{BB_t}}\right|_{\mathrm{LWP}} = \left.\frac{\partial \ln \tau}{\partial \ln \mathrm{BB_t}}\right|_{\mathrm{LWP}} \quad (1)$$

The maximum value of ACI as derived from Eq. (1) is 0.33. An ACI value of 0.33 corresponds with the 1.0 maximum possible change in $\ln N_{\mathrm{liq}}$ relative to $\ln \mathrm{BB_t}$, which would occur if every aerosol were to nucleate a cloud droplet. The first term of Eq. (1) is divided by 3 in order to correspond with the last two terms, which are derived at constant LWP from the following theoretical relationships: $r_{\mathrm{e}} \propto \mathrm{LWP}/\tau$ (Stephens, 1978) and $\tau \propto N_{\mathrm{liq}}^{1/3}$ (Twomey, 1977). Note that although each term in Eq. (1) should equal each other term, in practice measurement-derived biases can cause apparent differences between the terms. This issue will be discussed further in later sections.

One study convincingly demonstrated that smoke reduces cloud droplet effective radius and enhances cloud albedo in Arctic liquid clouds (Tietze et al., 2011). In that study, modeled $\mathrm{BB_t}$ concentrations were combined with remote sensing of cloud properties, enabling the authors to reduce meteorological bias by basing their conclusions on tens of thousands of clouds sampled over a variety of meteorological conditions throughout the Arctic. Smoke ACI values derived from relative changes in cloud r_{e} were estimated at between 0.04–0.11 out of a maximum 0.33. (Note however that in that study, clouds were binned by temperature and pressure, rather than by LWP as in Eq. 1 above.)

However, despite being able to conclusively demonstrate a smoke cloud albedo effect, Tietze et al. (2011) noted that they might have underestimated the magnitude of satellite-derived ACI values because of difficulties constraining aerosol concentrations and locations. They cite a study by Costantino and Breón (2010), where it was demonstrated that not co-locating aerosol-cloud layers in the vertical column dramatically lowered ACI estimates from 0.24 to 0.04 over marine stratocumulus clouds influenced by African biomass burning. This bias seems to be apparent in many ACI estimates globally; from a literature search, McComiskey and Feingold (2012) revealed

ACPD
15, 22823–22887, 2015

that remote sensing-derived ACI values worldwide are lower than those derived from in-situ, modeling and/or ground-based studies. They also showed that in addition to errors in co-location of clouds and aerosols, the comparatively low spatial resolution of remote sensing observations can further enhance the low bias in ACI estimates.

In the Arctic, these biases can be substantial. In a study in Northern Finland, ACI estimates derived over the same general time period and location from both ground-based and remote sensing methods were ~ 0.25 and 0.09 ± 0.04, respectively (Lihavainen et al., 2010); a more than two-fold difference. For reference, the range of Arctic remote sensing-derived ACI estimates for all aerosol sources is -0.01 to 0.09 (Lihavainen et al., 2010; Tietze et al., 2011); in situ, ground-based, and model estimates range between 0.05–0.3 (Garrett et al., 2004; Lihavainen et al., 2010; Zhao et al., 2012). The degree of bias at other global sites has led McComiskey et al. (2012) to assert that the albedo effect can only be assessed accurately from aircraft or ground-based in situ data.

To better understand the impacts that expected increases in smoke will have on the Arctic, it is important to better constrain remote-sensing and model estimates of smoke-specific ACI in the Arctic using in situ aircraft data. The biggest challenge in obtaining representative aircraft-based ACI values is the fact that they are more prone to uncertainties caused by the influences of poorly constrained meteorological factors (Shao and Liu, 2006) than other methods due to logistical limitations in sample size. We confront this issue in two ways. First, we focus on a case study day from the Arctic Research of the Composition of the Troposphere from Aircraft and Satellites (ARCTAS) campaign (Fuelberg et al., 2010; Jacob et al., 2010) in which several clouds were sampled under very similar conditions. We derive ACI estimates for all clouds that were either verifiably clean or are clearly influenced by biomass burning aerosols, and contrast the observed cloud properties. Second, to increase sample size, we consolidated data from four separate aircraft campaigns in the Arctic. In addition to ARCTAS, these datasets include: the First ISCCP (International Satellite Cloud Climatology Project) Regional Experiment Arctic Clouds Experiment (FIRE.ACE), which included portions

ACPD
15, 22823–22887, 2015

flown by the University of Washington Convair-580 (UW FIRE.ACE) and the Canadian National Research Council Convair-580 (NRC FIRE.ACE) (Curry et al., 2000), and the Indirect and Semi-Direct Aerosol Campaign (ISDAC) (McFarquhar et al., 2011). We then compare these findings with those from the ARCTAS case study.

2 Methods

2.1 Dataset description

The dates and flight locations of data used in this study are shown in Fig. 1, and the data used are listed in Tables 1–4. The ARCTAS, FIRE.ACE, and ISDAC datasets have each been extensively described previously (e.g., Curry et al., 2000; Fuelberg et al., 2010; Jacob et al., 2010; Korolev et al., 2003; McFarquhar et al., 2011; Rangno and Hobbs, 2001; Soja et al., 2008). However, to our knowledge, they have never been compared directly to each other. Here we note only briefly a few relevant points about the datasets and how they are inter-compared.

First, during the ISDAC and FIRE.ACE flights, multiple passes inside clouds were often obtained, and aerosols were intentionally sampled above- and below-cloud. In contrast, during ARCTAS there was very limited resampling of a given region and generally only one pass through a cloud was obtained. This difference in sampling impacts our results only in that there are not as many vertical profiles through the ARCTAS clouds as in the other datasets. Second, the UW FIRE.ACE dataset contains some gaps in positional data (latitude, longitude, and altitude), which range most frequently between 1–10 s, with rare instances of gaps > 1 min. If the data were out-of-cloud and if the gap in positional data is < 1 min, we linearly interpolate the latitude, longitude, and/or altitude. Otherwise, occasional gaps > 1 min and data without positional information were excluded. Thirdly and most importantly, we have made our best effort to use data that are as comparable as possible between campaigns. However, when high quality measurements are not available from the same instrument in all campaigns,

ACPD
15, 22823–22887, 2015

we use the most similar measurement available and we discuss the uncertainties this raises in the text.

2.2 Cloud presence and phase

2.2.1 ARCTAS

In ARCTAS, cloud liquid water content (LWC) was determined from droplet size spectra gathered with the CAPS-CAS instrument (Baumgardner et al., 2001) for particles 0.5–50 µm in diameter. Liquid phase cloud presence was defined by LWC values $\geq 0.01\,g\,m^{-3}$ (Matsui et al., 2011b), a value that corresponds well with cloud presence verified from the on-flight video. Because neither ice water content (IWC) nor cloud particle images were directly measured during ARCTAS, we are unable to accurately verify cloud phase at temperatures < 0 °C in the ARCTAS dataset. Therefore, we limited our focus within the ARCTAS dataset to clouds present at temperatures > −0.5 °C (i.e., those clouds highly likely to be in the liquid phase). We also excluded clouds that video indicated were affected by drizzle or ice precipitation from cloud layers above.

2.2.2 FIRE.ACE and ISDAC

During the FIRE.ACE campaigns, LWC was determined from droplet size spectra gathered from Forward Scattering Spectrometer Probe (FSSP-100) measurements for particles with diameters between 0.5–47 µm. These measurements are functionally very similar to the CAPS CAS measurements from ARCTAS. At LWC values $< 0.5\,g\,m^{-3}$ (in non-drizzling conditions) FSSP data had a close relationship to hot-wire probe measurements of LWC, although the absolute value of LWC was lower (Table 5). During ISDAC, LWC was determined from cloud droplet probe (CDP) data. These data agreed within 15 % of the bulk probe values. Following Earle et al. (2011), Forward Scattering Spectrometer Probe (FSSP) data were used on days when high-quality CDP data were unavailable; the FSSP data are estimated to agree with CDP data to within 20 %.

ACPD
15, 22823–22887, 2015

For comparability with ARCTAS clouds, the presence of liquid clouds in the FIRE.ACE and ISDAC datasets was determined by simultaneous measurements of LWC $> 0.01\,g\,m^{-3}$. Also, for inter-campaign comparisons we focused on clouds sampled for $\geq 20\,s$ in order both to increase representativeness of the average measured properties of the clouds and to enhance meteorological similarity of clouds. Sometimes entrainment from outside air caused pockets of low- to no-LWC (i.e., LWC $< 0.001\,g\,m^{-3}$) within a cloud body; these pockets of air were not included when determining the average cloud droplet effective radius.

There is no consistent definition for cloud phase in the literature. In remote sensing studies for example, cloud phase is usually determined by cloud radiative properties – thus, clouds with some mixed particles can be included in "liquid" or "ice" phase classifications if they are mostly liquid or mostly ice (e.g., Baum et al., 2012; Platnick et al., 2003). Due to instrumentation limitations, aircraft studies sometimes also define a cloud with small fractions of ice particles as being a "liquid" cloud (e.g., Korolev et al., 2003). Alternatively, distinct portions of a cloud may be classified as different phases if a primarily liquid portion of a cloud is far away ($\sim$ 1–2 km) from a mixed portion of a cloud mass (McFarquhar et al., 2007; Zuidema et al., 2005).

Here, we define liquid cloud phase by the lack of any ice particles in the CPI data throughout the entire cloud transect, based on a roundness criterion (Lawson et al., 2001). When possible (i.e., in the NRC FIRE.ACE and ISDAC datasets), we verified that there was no detectable ice water along the cloud transects. This relatively stringent definition of liquid phase clouds is used to describe as best as possible the liquid phase end-member cloud characteristics. Because aircraft cloud transects can only sample a portion of a cloud, we must assume that the portion of the cloud sampled is representative of the rest of the cloud. This may introduce uncertainties, particularly in persistent large-scale stratus clouds. Nonetheless, as discussed in Sect. 3.1, we believe that errors from this assumption are not likely to have a large impact on our results.

ACPD
15, 22823–22887, 2015

2.3 Cloud microphysical properties

We used aircraft vertical profiles to assess cloud droplet effective radius (r_e), cloud liquid water path (LWP) and cloud optical depth (τ), and to gather information on aerosol properties above and below cloud. The r_e was derived by Eq. (2), following Hansen and Travis (1974):

$$r_e = \frac{\int r^3 n(r)\,\mathrm{d}r}{\int r^2 n(r)\,\mathrm{d}r} \tag{2}$$

where r is the radius variable, and $n(r)$ is the cloud particle size distribution. LWP is defined as the vertical integral of LWC from the base to the top of the cloud. LWP values were only determined when vertical profiles through the cloud were available, thus providing the cloud base and top heights. We define τ following Peng et al. (2002) as:

$$\tau = \frac{3}{2}\frac{\mathrm{LWC}H_c}{r_e \rho_w} \tag{3}$$

where H_c is cloud thickness (again only available in vertical cloud transects) and ρ_w is the density of water. In addition to vertical transects, we also used horizontal transects within clouds to obtain information on horizontal variability of within-cloud properties and to obtain increased sample numbers for r_e.

In some instances in the multiple-campaign analysis, the same cloud or very similar clouds were sampled more than once, often intentionally, either through an entire vertical cloud transect or through a portion of a cloud. In order to reduce the potential for pseudo-replication in the analysis, transects that were deemed to be from the same cloud or from very similar clouds were averaged to provide one aggregated profile or r_e and N_{liq} value for those instances. Clouds were determined as being related in part by a combination of time and location sampled. Here, the range of distance and time between clouds deemed as related or the same ranged from 0.4–76 km and several

ACPD
15, 22823–22887, 2015

seconds to 2.5 h apart, depending on the conditions and cloud type (the 2.5 h time frame included 8 separate transects through a stratus cloud). In addition, we assessed cloud pressure, location, temperature, on-flight video (when available), and, in biomass burning cases, nearby aerosol conditions (as determined by CH_3CN, black carbon, BC, submicron SO_4^{2-} and submicron organic aerosol, OA, concentrations in the ARCTAS, and SPLAT II number composition the ISDAC). Within the multi-campaign analysis, 2 of the 8 biomass burning clouds contained aggregated transects, as did 5 of the 16 background clouds. One background cloud in the case study included aggregated transects. LWC among aggregated clouds was generally similar (within 30 % of each other), but in some cases it was more variable (in one biomass burning aggregation, the set of 8 related cloud transects had LWCs ranging 0.12–0.54 g m^{-3}). To assess the impact of cloud transect aggregation on our analysis, we calculated differences in ACI values using the maximum and minimum values of N_d within the aggregated samples. Calculated differences in ACI values were 1 %, indicating that uncertainties caused by aggregation had only minor impacts on our results.

2.4 Air mass classification

For this work, distinguishing smoke-influenced from background cloud conditions is critical. During ARCTAS, background conditions were selected by a combination of in-cloud gas concentrations (average CO < 123 ppbv and average acetonitrile (CH_3CN) < 0.14 ppbv) and near-cloud SO_4^{2-} and BC concentrations (< 0.9 µg m^{-3} and < 0.3 µg C m^{-3}, respectively). In ideal cases, "near-cloud" air masses were defined as half the width of the cloud if it was a vertical profile, and within 10 s before and after the cloud if it was a horizontal transect. However, sometimes the presence of a neighboring cloud or the vertical changes in the aircraft track forced us to use slightly smaller samples. The 123 ppbv CO cutoff value represents the upper quartile range of time periods with concurrently low CO, CH_3CN, and BC (all separate indicators of combustion), and the CH_3CN cutoff is the median for these values. For comparison,

ACPD
15, 22823–22887, 2015

Lathem et al. (2013) and Moore et al. (2011) defined background air masses as having CO and CH_3CN values at < 170 and 0.1 ppbv, respectively, and Lance et al. (2011) used a criterion of ∼ 160 ppbv CO. ARCTAS "biomass burning" influenced air masses were classified following the procedure of Lathem et al. (2013), where BB-influenced air masses have concentrations of > 175 ppbv and 0.2 ppbv CO and CH_3CN, respectively. For comparison, Lance et al. (2011) used a concentration of > 200 CO for "polluted" (mostly biomass burning) cases.

During the two FIRE.ACE campaigns, high quality aircraft chemical data for completely characterizing air mass sources were not collected, and remote sensing products useful for air mass classification were also unavailable. As a result, biomass burning-derived haze events were indistinguishable from anthropogenic pollution events in the FIRE.ACE datasets. Therefore, we only use FIRE.ACE clouds sampled under non-polluted background conditions for inter-comparison with the other datasets.

Because within-cloud gas concentrations were not available, we used average near-cloud (as defined above) aerosol concentrations to define "background" conditions in the FIRE.ACE data. To reduce the risk of any potential humidification effects, we excluded near-cloud air masses that had any observations of cloud particles in the CPI or that had LWC values $\geq 0.001\ g\ m^{-3}$.

To be classified as background, air masses directly adjacent to the cloud had to have Passive Cavity Aerosol Spectrometer Probe (PCASP) aerosol concentrations (CN_{PCASP}) ≤ 127 particles cm^{-3} (Shantz et al., 2012). The PCASP measures dehumidified particles with diameters between 0.12–3 µm. This CN_{PCASP} cutoff is a more stringent criterion for determining clean conditions than those adopted by Jackson et al. (2012), Earle et al. (2011) and Peng et al. (2002), where respective values of < 200, 250 and 300 particles cm^{-3} were used, but the criterion applied here appears to exclude biomass burning and pollution aerosols fairly effectively (Table 6). However, the upper 95 % CH_3CN concentrations are higher than typical background conditions, indicating that our chosen cutoff value is generally, but not completely, effective at removing air masses influenced by smoke. Therefore, the FIRE.ACE samples have a more un-

ACPD
15, 22823–22887, 2015

certain background classification than the ARCTAS and ISDAC datasets, where actual chemical tracers verify the presence of pollution and biomass burning aerosols.

For ISDAC samples, "background" conditions were determined by out-of-cloud CN_{PCASP} concentrations, in order to be consistent with the FIRE.ACE campaigns. However, the TSI aerosol concentrations (CN_{TSI}) and backscatter values were not used to assign a background classification (see Sect. 3.2 for further details).

A "biomass burning" classification was assigned in ISDAC data when a cloud had contact with discernable amounts of biomass burning aerosols, as determined by single particle mass spectrometer, SPLAT II (Zelenyuk et al. 2009, 2015), based on the mass spectral analysis of individual aerosol particles (Fig. 2). This method has been similarly employed to determine biomass burning influence in the ISDAC dataset previously (Earle et al., 2011; McFarquhar et al., 2011; Shantz et al., 2014).

2.5 Assessment of indirect effects from biomass burning

As mentioned before, the impact of smoke aerosols on cloud droplet activation was assessed by looking at aerosol-cloud interactions (ACI) of biomass burning aerosols on cloud droplet number. The ACI values were derived from changes in cloud droplet number relative to measured biomass burning tracers, BB_t, following Eq. (1) and using a non-parametric Kendall robust line-fit method (see Appendix A for details).

As previously mentioned, ARCTAS was the only campaign where biomass burning gaseous tracers were directly quantifiable in-cloud (here we use $BB_t = CH_3CN$, de Gouw et al., 2003, and $BB_t = CO$, Tietze et al., 2011), measured in ppbv. Both CO (Bian et al., 2013) and CH_3CN have appreciable background concentrations in the Arctic (as can be seen in Fig. 3a). Therefore, approximate background CO and CH_3CN concentrations of 99.2 and 0.088 ppbv, respectively, were subtracted prior to deriving ACI values from Eq. (1) in the case study. These background values were derived from the mean of the Kendall robust line-fit method analyses of ARCTAS CCN and CN_{PCASP} equivalent concentrations vs. CO (or CH_3CN) concentrations. In the multi-campaign analysis, background values of 0.018 were subtracted, due to lower background con-

ACPD
15, 22823–22887, 2015

centrations in the cleanest samples. Although for simplicity we define a single background Arctic CH_3CN level here, background CH_3CN can range from ∼ 0.050 ppbv in the Arctic marine boundary layer to ∼ 0.1 ppbv at altitudes of ∼ 8 km (A. Wisthaler, personal communication, 2015). A maximum error of 0.038 ppbv in background CH_3CN would equal at most 18 % of the CH_3CN signal in biomass burning samples. For that reason, and because CH_3CN was only one of six tracers used to derive ACI values, the range of possible background CH_3CN concentrations is expected to have only minor impacts on the analysis. Arctic background CO is more consistent than CH_3CN, and in that case, the differences in background CO as computed from CN_{PCASP} vs. CCN line-fit analyses (93.0 and 105.4 ppbv, respectively) led to only a 2.6 % change in the derived ACI values.

Because the in-cloud CO and CH_3CN values were not available in the ISDAC or FIRE.ACE campaigns, we also compared aerosol tracers of smoke/polluted particles adjacent to the cloud as a BB_t quantity. The aerosol tracers used were CN_{PCASP} concentrations, backscatter at 550 nm, BC concentrations, and when available, CCN (not available in the UW FIRE.ACE campaign). For comparison to the PCASP, aerosol concentrations with diameters > 4 nm were measured with a TSI 3775 in ISDAC. Aerosols with diameters > 3 and 10 nm were measured during ARCTAS from TSI models 3025 and 3010, respectively. Because CN_{PCASP} values were not measured during ARCTAS, we combined APS and UHSAS sized aerosol data collected during that campaign into a similar size distribution as the CN_{PCASP} measurements (0.124–3.278 µm). UHSAS and APS measurements are not actively dried like PCASP samples are (Earle et al., 2011; Strapp et al., 1992), but sample humidity decreases significantly upon heating in the cabin and measurements are taken at dry relative humidity.

There are some limitations of the ACI approach. First, a systematic bias can be introduced when aerosol and cloud properties are averaged or co-located in low spatial or temporal resolution datasets (McComiskey and Feingold, 2012). This particular systematic bias is generally not a large concern for in-cloud aircraft studies such as this one where gas and/or aerosol measurements and N_{liq} measurements are either col-

ACPD
15, 22823–22887, 2015

lected simultaneously or in very close proximity. Secondly, the magnitudes of derived ACI can vary depending on the BB_t tracers used. To minimize the associated uncertainty, we use a combination of up to six BB_t tracers to derive ACI, as available.

A third potential problem is the risk that a snapshot of a cloud in time is not representative of the net cloud properties over its lifetime (Duong et al., 2011). This source of sampling error can only be fully eliminated in model simulations, and it is best minimized in aircraft in situ data by resampling throughout the cloud's life cycle. Resampling was sometimes, but not always, carried out for individual cloud cases presented here, and was not specifically carried out throughout the lifetime of the cloud. However, based on the results presented in Duong et al. (2011), the magnitude of this type of error is unlikely to have a large impact on our results, although we cannot with full confidence assess how cloud life stage might have impacted the way aerosols were interacting with the clouds.

The fourth limitation with the ACI method is that N_{liq} has a sublinear relationship with CCN (Morales et al., 2011; Morales and Nenes, 2010), with particularly noticeable deviations from linear behavior expected when a cloud contains high CCN concentrations (Moore et al., 2013). This behavior is driven by increased competition for water vapor, which in turn decreases cloud supersaturation and reduces the tendency to form additional drops. Because ACI values are typically derived from linear-type regressions, apparent ACI values can be reduced if clouds with high CCN are included in the analysis. We discuss the potential for this type of interaction where applicable in the text. Finally, the most difficult problem to address is the potential bias introduced if one does not account for meteorological conditions (Shao and Liu, 2006). We discuss the relationship of derived ACI with meteorology in the text below.

2.6 Overview of surface and meteorological conditions

Ambient conditions such as cloud type and presence of drizzle from an overlying cloud deck were determined from available video, photos, flight notes and AVHRR images. Although in situ chemical and physical measurements were primarily used to determine

ACPD
15, 22823–22887, 2015

end-member situations (i.e., where only smoke or only background air were the dominant sources of aerosols interacting with clouds), in some cases we discuss out-of-cloud aerosols with potentially more mixed sources. In these cases we supplemented chemical and physical data with 5-day HYSPLIT back trajectories (Draxler, R. R. and Rolph, G. D. HYSPLIT, HYbrid Single-Particle Lagrangian Integrated Trajectory, Model access via NOAA ARL READY Website, http://www.arl.noaa.gov/HYSPLIT.php, NOAA Air Resources Laboratory, College Park, MD) to determine recent air mass history. Using video, photos, and flight notes, clouds were also classified as either stratiform or cumuliform. Stratiform clouds were present at 1–3 km altitude. With one exception (an ARCTAS-B background case from 8 July 2008), the stratiform clouds were not present below a temperature or moisture inversion. In our dataset, none of the biomass burning cases were present below an inversion either; such inversions occurred only in four of the clean background cases, indicating generally unimpeded aerosol mixing from above and below for biomass burning clouds in these data. The cumuliform clouds were also found between 1 and 3 km, and although they were less optically thick than the stratiform clouds, optically thin ($\tau < 15$) and multi-layer clouds dominated all samples.

Across all clouds sampled during the four campaigns, there was substantial variation between clouds, as shown by the temperature and specific humidity profiles (Table 7) and the physical locations of the clouds (Fig. 4). For example, background clouds were primarily sampled over open-ocean and at higher latitudes, whereas the smoky clouds were primarily sampled at lower latitudes over land. For this reason, in addition to comparing median characteristics of all background and clean cases, we also focus on a case study where multiple clean and smoky clouds were observed under very similar meteorological and surface conditions (see below).

ACPD
15, 22823–22887, 2015

3 Results

3.1 Indirect effects of smoke in Arctic liquid phase clouds

On 1 July 2008 during the ARCTAS-B campaign, a variety of small cumuliform clouds were sampled during flight 18 over inland Saskatchewan, Canada. The physical characteristics of the clouds were very similar (Table 8), being small (~ 0.7 km high, and ~ 0.2–7 km wide) non-precipitating clouds present between 1680 and 2650 m altitude, and far from any major temperature or water vapor inversions. All clouds were liquid phase, with low median LWC values of 0.02 g m^{-3} (the implications of which is discussed further down). All clouds had temperatures ranging from −0.1 to 3.1 °C. All were sampled within 97 km^2 and 5.2 h of each other, during which time each cloud experienced similar northeasterly wind direction.

Despite being exposed to similar meteorological and surface conditions, aerosol inputs to these clouds ranged significantly, with average CH_3CN and PCASP equivalent particle numbers ranging between 0.092–0.55 ppbv and 107–3001 cm^{-3}, respectively. The large range in chemical properties was due to the aircraft track, which repeatedly covered areas up- and downwind of local fresh smoke plumes from the Lake McKay fire. This fire is comprehensively described in the combination of Cubison et al. (2011), Alvarado et al. (2010), and Raatikainen et al. (2012).

In Fig. 3, we show that out-of-plume CO (CO < 500 ppbv) is strongly related to the smoke tracer CH_3CN and that it shows no correlation to the fossil fuel combustion tracer dichloromethane (CH_2Cl_2) (see Kondo et al., 2011, for further discussion on use of this tracer during ARCTAS). Given that CO has both pollution and biomass burning sources, this finding indicates smoke was the dominant aerosol contributor on that day, not pollution. Back trajectories also support this conclusion (Alvarado et al., 2010). Of the clouds sampled during this flight, two clouds met the classification criteria for being biomass burning influenced, three were classified as intermediate, and three met the ARCTAS background criteria.

ACPD
15, 22823–22887, 2015

As shown in Fig. 5, smoke is clearly correlated with reduced cloud droplet radius in the eight clouds studied (with a median 51 % reduction relative to background clouds, Table 8). As expected, there was a concurrent increase in cloud droplet number (Fig. 5). Based on this increase, we compute a combined median ACI of 0.06 (bootstrapped 95 % confidence interval 0.05–0.07) across all tracers shown in Fig. 5.

Although linear regressions were not used to derive ACIs, we plot them for each tracer in Fig. 5 to show the degree of variation between individual tracer ACI values. Other researchers have previously noted differences in calculated ACIs when these interactions are computed from different tracers (e.g., McComiskey et al., 2009, Lihavainen et al., 2010, and Zhao et al., 2012), and these differences probably reflect a combination of measurement error and how well a given tracer approximates the subpopulation of aerosols that are participating in cloud droplet activation (Lihavainen et al., 2010). As plumes age, there may also be increasing uncertainty in biomass burning aerosol co-location with gaseous tracers such as CO and CH_3CN, as these are subject to different depositional processes (Hecobian et al., 2011). However, in this case the fires were relatively fresh so this issue is unlikely to be an important source of uncertainty.

ACI estimates can also sometimes be influenced or even overwhelmed by systematic differences in local meteorological conditions associated with cleaner versus more polluted clouds (Hegg et al., 2007; Shao and Liu, 2006). For the case study, that possibility is unlikely because of the relatively small area and time frame considered and the similar meteorological conditions in which the clouds were sampled.

However, because case study smoky clouds had a combination of very low LWC, very high aerosol concentrations from a fresh fire, and consequently, very small droplet sizes (Fig. 6), it is likely that smoky case study clouds were less sensitive to further additions of smoke aerosols than clouds with lower aerosol concentrations. Such nonlinear behavior is predicted when high CCN levels cause increased competition for water vapor, which in turn decreases cloud supersaturation and reduces the tendency to form additional drops (Moore et al., 2013; Morales et al., 2011; Morales and Nenes,

ACPD
15, 22823–22887, 2015

2010). Additionally, possible enhanced entrainment of outside air in smoky clouds compared to background clouds (Ackerman et al., 2004; Bretherton et al., 2007; Chen et al., 2012; Lebsock et al., 2008) could enhance droplet evaporation and further reduce ACI values from the expected adiabatic ACI maximum value at a given aerosol level.

Because in-situ ACI derivations assume linearity in the response of N_{liq} to BB_t, and such as assumption does not hold well at high CCN levels, we would expect to derive lower in-situ ACI estimates if clouds with very high CCN levels are included in the analysis (Rosenfeld et al., 2014). That ACI values would increase to 0.08 (95 % confidence interval 0.05–0.15) if the two biomass burning clouds were excluded suggests that non-linear processes were indeed affecting the reduced ACI values in the case study. For reference, at case study smoky CN_{PCASP} equivalent concentrations of $\sim$2000–3000 cm^{-3}, modeled adiabatic ACI values were $\sim$0.06–0.16 (Moore et al., 2013). The range in modeled ACI values depended on factors such as cloud vertical velocity and CCN hygroscopicity (the CCN spectrum). Given these model uncertainties and our estimated case study ACI value, any potential effects of entrainment were not clearly noticeable in our data.

For these reasons, although the 1 July 2008 case is in some ways ideal in that the clouds were sampled in very similar environmental conditions, it is not necessarily representative of typical cloud conditions in the Arctic. The clouds were present relatively far south in the subarctic (52–56° N) and were cumuliform compared to the more dominant Arctic stratus type clouds. Moreover, the case study clouds were subjected to fresh concentrated smoke rather than aged diluted smoke, as one would expect at higher latitudes. Therefore, as explained above, we expect case study clouds already affected by high smoke concentrations to have reduced sensitivity to additional smoke, particularly given the low LWC of the case study clouds.

To assess the impact of smoke on liquid clouds more generally, we compared background and biomass burning cloud properties sampled over the larger region shown in Fig. 4. This more expansive set of clouds includes a broader range of high-latitude meteorological conditions, making it more representative of overall conditions in the Arctic

ACPD
15, 22823–22887, 2015

region. However, the greater heterogeneity also makes trends in the data more difficult to interpret, as we cannot describe in full detail the degree to which meteorological influences affected each cloud given the limitations of the datasets.

Despite the uncertain meteorological influence, we see qualitatively similar trends to those in the 1 July 2008 ARCTAS case study (Fig. 7). We find a 4.6 µm (57 %) median reduction in r_e between the smoky and background cases (Table 7). Concurrently, median N_{liq} increased from 38 droplets cm^{-3} in background clouds to 321 droplets cm^{-3} in smoky clouds. Within stratiform-only and cumuliform-only liquid clouds, groupings that are somewhat more comparable meteorologically, the mean r_e differences are 2.7 and 5.6 µm (n = 6 and 14), respectively. However, the combined median ACI estimate from all tracers shown in Fig. 7 is 0.12 (95 % confidence interval 0.10–0.13). This value is double that of the case study, which is further evidence to suggest that cloud sensitivity to aerosols in the case study was lowered by aerosol-driven adiabatic reductions in cloud supersaturation (and possibly enhanced entrainment).

Observed smoke-driven reductions in liquid cloud droplet size and increases in cloud droplet number in both the case study and the multi-campaign analysis are in line with several other studies in the Arctic. Peng et al. (2002) found a nearly identical difference in r_e of 4.8 µm to the multi-campaign analysis in two combined datasets in the Arctic (one of which was the NRC FIRE.ACE dataset), in conditions where PCASP values were > and < 300 particles cm^{-3}, although they did not specifically focus on biomass burning-related samples. Tietze et al. (2011) also found significant changes in LWP, τ, and r_e using remote sensing cloud observations combined with a modeled biomass burning tracer. In contrast, Earle et al. (2011) did not see a reduction in r_e in biomass burning-influenced clouds based on selected ISDAC samples. They attributed this finding to a combination of meteorological and microphysical factors. It is possible that some of the differences with our study are also caused by reduced contrast between selected clean and polluted cases, as their cutoff for defining clean conditions was higher than ours, and they did not include any samples that met our background criteria (which were only present during the 4 April 2008 ISDAC flight). Also note that

ACPD
15, 22823–22887, 2015

the biomass burning-influenced cloud cases assessed by Earle et al. (2011) did not overlap with the clouds assessed in this study.

As noted previously, because the aircraft could only sample transects of clouds, we had to assume that the observed cloud phase was representative of the whole cloud. In the case study, all clouds were sampled at temperatures > 0 °C, and this assumption holds well. In Arctic stratocumulus clouds, ice is typically well mixed throughout (McFarquhar et al., 2007, 2011). Where we expect this assumption to be most uncertain is in stratiform clouds in the multi-campaign analysis, which might have different properties in far-off, non-sampled portions. Uncertainties are also higher in clouds that were only transected horizontally, because mixed phase clouds in the Arctic frequently have vertical layers of ice and liquid particles (Morrison et al., 2012). We cannot fully rule out that non-sampled portions of the clouds in the multi-campaign analysis contained ice particles, or that different vertical layers had different r_e values. However, if the 6 ISDAC and FIRE.ACE background clouds that were either stratiform or that contained only horizontal transects are excluded, the results of the multi-campaign analysis are nearly the same (ACI = 0.12 and median background cloud r_e = 8.3 vs. 8.1 µm). Thus we do not believe that uncertainties in cloud phase had a major impact on our results.

3.2 Implications for radiation and precipitation

Based on model output by McComiskey et al. (2008) (their Fig. 2a), we estimate that given the case study median ACI value of 0.06, the smoke-derived cloud albedo effect on radiative forcing could be ∼ −2 to −4 W m^{-2} for regions with surface albedo of ∼ 0.15. The McComiskey et al. (2008) output was based on the assumption of homogeneous, unbroken clouds with CCN concentrations of 600 cm^{-3}, a LWP of 50 g m^{-2}, and a cloud base height of 500 m. Such surface albedo and cloud/aerosol conditions are similar to some of the summer terrestrial conditions sampled over Canada during ARCTAS-B. The summer subarctic biomass burning clouds we describe from ARCTAS-B CCN and LWP levels bracket the model's assumptions, ranging between 1–94 g m^{-2} and 68–6670 cm^{-3}, respectively. However, cloud base heights were typically higher

ACPD
15, 22823–22887, 2015

than the model assumed-500 m, and although unbroken clouds are observed there, the ACI value we use was determined in a broken cloud system. Periodic broken cloud conditions, cloud heterogeneity (McComiskey et al., 2008), and the patchiness of smoke will all reduce the net cloud albedo radiative forcing over wider spaces and times. Therefore, the -2 to $-4\,W\,m^{-2}$ range is only applicable in the subarctic in some conditions. Nonetheless, this estimate at least provides a rough indication of how important these effects might be.

In contrast to the subarctic, in the Arctic high surface albedo will lessen the expected impact of the cloud albedo effect. Although future sea ice losses and associated reductions in surface albedo may affect the relative importance of the cloud albedo effect on Arctic clouds, others (e.g., Garret et al., 2004) have suggested that in the Arctic, a more important impact of reduced cloud droplet size may be greater longwave opacity, which can lead to enhanced snow melt. Relatedly, smaller droplets may affect cloud lifetime either by extending it via reduced precipitation (the "second indirect effect"; Ackerman et al., 2000; Albrecht, 1989) or by reducing it via enhanced water vapor competition and evaporation, as may have occurred in the case study.

Cloud droplet spectra from the 1 July 2008 ARCTAS case study clouds are shown in Fig. 6. Although sample size is small, the presence of smoke appears to narrow the droplet spectra from a dispersion of 0.82 in background clouds to 0.54 in smoky clouds, as calculated by the ratio between the standard deviation of the size distribution and the mean droplet radius. This narrowing is likely to lessen the eventual probability of coagulation (Tao et al., 2012), as is moves median droplet size further away from the 28 µm effective diameter threshold at which collision/coagulation processes are thought to become efficient enough to induce precipitation (Rosenfeld et al., 2012).

Cloud droplet spectra from the multi-campaign clouds are shown for comparison in Fig. 8. There is not as obvious a narrowing of spectra as for the case study, but droplet concentrations with 28+ µm diameters were several orders of magnitude lower in smoky vs. background clouds (Fig. 8). Also, small droplet concentrations (those most susceptible to evaporation) increased, and rainfall was only noted in clean conditions,

ACPD
15, 22823–22887, 2015

as shown in Fig. 8 by elevated ($>0.1\,cm^{-3}$) cloud droplet concentrations with diameters $>50\,\mu m$ (King et al., 2013). Therefore, although clouds outside the case study suffer large uncertainties related to their collection over heterogeneous conditions, their droplet distributions support the hypothesis of smoke-induced reductions in drizzle.

3.3 Interactions of biomass burning particles with background aerosols – potential impacts on clouds

Previous authors have noted the presence of large numbers of small, low-scattering Aitken particles in the Arctic (Garrett et al., 2004; Howell et al., 2014; Leck and Bigg, 1999; Zhao and Garrett, 2015), which other studies have suggested may be marine in origin (Heintzenberg et al., 2006; Karl et al., 2012; Leck and Bigg, 1999; Orellana et al., 2011). New particle formation may be another source of the high Aitken particle number; marine processes can also be a substantial source of new particles (e.g., Allan et al., 2015). Either way, chemical data from the ARCTAS dataset (shown in Fig. 9), confirm that these Aitken particles were numerous and that they appear to have a natural background source.

Fortunately, the relatively large minimum size cutoff of the PCASP ($\sim 120\,nm$) excludes these background particles (Fig. 10), and the CN_{PCASP} concentration seems to accurately indicate the presence of particles from pollution and biomass burning sources (Figs. 9 and 10), independent of whether small background aerosols are present. This finding is in-line with previous studies that found low altitude Arctic biomass burning aerosols primarily in the accumulation mode (Earle et al., 2011; Warneke et al., 2010) and other studies that found the peak size of marine background particles to be between 25–80 nm (Leck and Bigg, 2005).

However, although the PCASP seems to effectively exclude the individual small background aerosols, there is evidence to suggest that these background particles are interacting with the larger accumulation-mode biomass burning and pollution particles, and perhaps changing their properties. In Figs. 9 and 10, we plot all non-cloud high-quality

ACPD
15, 22823–22887, 2015

data from ARCTAS and ISDAC. These data from multiple air masses show that there are two distinct populations of aerosols: small particles in the clean background having low CO, CH_3CN, and backscatter, and larger, combustion-derived particles. In both campaigns there is a clear separation between low scattering background air masses and polluted air masses.

Two possibilities could explain the dual distributions. First, it is possible that two separate air masses were observed that did not passively mix during the sampling periods (otherwise we would expect passive mixing to blur together the two distributions observed in Figs. 9 and 10). Another possibility is that the small background particles were coagulating onto larger aerosols when air masses having different aerosol sources came into contact.

At first, the larger scatter in aerosol-backscatter optical properties in ARCTAS-B samples compared to ARCTAS-A suggested the distribution was caused by two non-mixing separate air masses, as did the fact that most days were characterized by either all small, weakly scattering particles, or all larger, scattering particles. However, upon closer analysis, it seems that the greater range in backscatter at a given CN concentration in ARCTAS-B is more likely caused by differences in smoke optical properties. Most of the ARCTAS-B samples with backscatter $>2.5\,Mm^{-1}$, and with a high relative particle number compared to ARCTAS-A at a given backscatter level were from fresh Lake McKay smoke samples on 1 July 2008 (Fig. 9, bottom row). Previous work has shown that these plumes were evolving, with ongoing evaporation of primary smoke particles and formation of secondary smoke particles (Cubison et al., 2010). Those resulting changes likely explain the large range in particle number at high backscatter levels in the fresh plumes from that day. Also, despite the scatter in the ARCTAS-B samples shown in Fig. 9, there was still separation between low scattering background air masses and polluted air masses, as there was in ARCTAS-A and ISDAC.

To better understand the reason for the dual distributions in Figs. 9 and 10, we focused on a few cases when aerosol properties transitioned as the aircraft moved between clean and polluted air masses. On 1 July 2008 (downwind of the ARCTAS-B

ACPD
15, 22823–22887, 2015

biomass burning case study) for example, the aircraft passed through several smoky haze layers into a clean air mass (Fig. 11). Both video and differential absorption LIDAR (DIAL) data confirm that the presence of the upper haze layer at 3–5 km was geographically widespread (Fig. 12). During the transition into cleaner air, CN_{TSI} number rapidly increased by ~ 1400 particles cm^{-3} within a 63 m vertical transition zone, and these particles were found to be fairly small (Fig. 11). Such a rapid change in CN_{TSI} concentrations could be explained by either a sharp non-mixing transition zone or by rapid coagulation of the small particles onto the larger haze particles.

As shown in Fig. 11c, there were some weak temperature and moisture inversions that might have inhibited mixing of these air masses to some degree (Fig. 11c). However, at the transition zone, both backscatter and OA concentrations changed at a much slower rate than the CN_{TSI} concentrations (Fig. 11), suggesting that mixing was in fact taking place over a broader scale. Although data were not available in the exact time period of interest, DIAL data taken shortly after the transition also suggest that the smoke layer was probably undergoing broad diffuse mixing (Fig. 12). In addition, despite the fact that high quality data were unavailable for size classifications < 0.5 µm diameter, it is clear that large particles contributed a higher relative percentage in the polluted layers than in the clean air mass (Fig. 11b), which is what we would expect if coagulation were occurring. Although not definitive, these observations suggest that coagulation was occurring during mixing.

Similar observations were made during a transect over the Bering Strait on 12 April 2008 (Fig. 13), when the airplane passed through a clean region with high CN_{TSI} and low backscatter sandwiched between two more polluted layers with higher CN_{TSI} and backscatter. Unfortunately, size distributions of particles with diameters < 0.5 µm were unavailable during this portion of the transect as well, but the available data indicate that there was again a higher fraction of larger particles in the polluted air masses (Fig. 13b). On either side of the clean air mass, submicron SO_4^{2-} concentrations began to rise, which back trajectories suggest was the result of transport from Asia. In the border regions, there was a sudden drop in CN_{TSI} of ~ 700–1000 particles cm^{-3} over

ACPD
15, 22823–22887, 2015

an ∼140 m vertical distance. As in the previous case, submicron SO_4^{2-} concentrations and backscatter also changed, but at a slower rate than CN_{TSI}. DIAL observations indicate that mixing of aerosols was occurring in a vertical zone of at least 500 m below the clean air mass.

If coagulation were occurring, it likely does not contribute to a large change in smoke aerosol volume during most smoke haze events. For example, we estimate that background aerosols could contribute only ∼1–4 % of the total smoke aerosol volume for smoke aerosols in the transition zone in the 1 July 2008 case presented in Fig. 11. (details on this calculation can be found in Appendix B). Although by volume this impact is fairly minor, Lohmann and Leck (2005) showed that marine-derived background particles are highly surface-active, and that they would likely activate at lower supersaturations than anthropogenic material or fresh smoke. Therefore, if these background particles act as surfactants or if they otherwise modify smoke CCN or IN characteristics, the coagulation of these particles onto larger smoke particles might impact cloud droplet formation or the way the presence of smoke affects cloud phase changes. These background particle effects would probably be largest in air masses with very diluted smoke and/or higher concentration background particles. For example, if concentrations of smoke from the above case were diluted by half (to ∼450 cm^{-3}) and background aerosol concentrations were doubled to ∼5000 cm^{-3} (these values are within the spread of data shown in Figs. 9 and 10), background aerosols could contribute up to 16 % of smoke aerosol volume if coagulation were to occur.

4 Discussion and Conclusions

The challenge of separating the influence of meteorology and aerosol indirect effects on clouds introduces relatively large uncertainty in our understanding of how smoke impacts clouds. Using in situ aircraft data, we quantified these impacts in both a subarctic cumulus cloud case study and in a multi-campaign data assessment of clouds north of 50° N. The multi-campaign assessment suggests an ACI value of 0.12 (95 %

ACPD
15, 22823–22887, 2015

confidence interval 0.10–0.13), which is on the high end of previous satellite-based assessments (0.04–0.11) (Tietze et al., 2011). Given a known low bias in remote-sensing-derived estimates of ACI (e.g., McComiskey et al., 2012), our findings suggest that smoke-derived increases in cloud albedo may be higher than previously derived in the region. We reduced confounding meteorological effects by including data from as wide a geographic region as possible, applying very stringent conditions to identify clean and smoky clouds, and reducing the impact of outliers on ACI derivations by using the Kendall robust line-fit method instead of normal linear regressions. However it is important to note that meteorological effects are still imperfectly constrained in this assessment due to inherent limitations in the in situ dataset size and content.

Therefore, for comparison, we also analyzed the 1 July 2008 ARCTAS case in the subarctic, where multiple clean and smoky clouds were found under similar meteorological conditions, and derived an ACI estimate of 0.06 (95 % confidence interval 0.05–0.07). The combination of low cloud LWC and high aerosol concentrations in the case study led to very small cloud droplets when smoke was introduced. Based on model results in Moore et al. (2013), these smaller droplets likely increased competition for water vapor; enhanced evaporation may also have occurred. Each process would limit the maximum magnitude of smoke cloud albedo effects. Therefore, we speculate that the 0.06 ACI case study value falls at the low-end of typical smoke ACI values for the larger subarctic/Arctic region.

Based on a previous model study by McComiskey et al. (2008), the ACI value of 0.06 from the case study suggests that smoke may reduce radiative flux via the cloud albedo effect by $\sim$2–4 W m^{-2} or more under certain conditions in the subarctic. At higher latitudes where surface albedo is already high, the impact on radiative flux is likely to be smaller. In those regions, a more important effect of smoke might be its inhibition of precipitation and cloud lifetime effect, as evidenced by the observed reductions in cloud droplet radius of $\sim$50 % in both the case study and the multi-campaign assessment.

Smaller cloud droplets can have various consequences. Smoke-driven reductions or delays in precipitation may affect the distribution of aerosol and moisture deposition.

ACPD
15, 22823–22887, 2015

Longer cloud lifetime could impact not only Arctic albedo but also longwave radiation (Stone, 1997), and previous studies suggest that even small changes in the above parameters may affect sensitive Arctic sea ice (Kay et al., 2008; Kay and Gettelman, 2009; Lubin and Vogelmann, 2006; Vavrus et al., 2010). Additionally, changes in cloud cover might also have indirect effects on ocean photosynthesis and biogeochemistry (Bélanger et al., 2013). It is our hope that the improved quantification of smoke-derived ACI values will help quantify these impacts in future model studies.

One obvious limitation of our study is that we do not address the impacts of smoke on existing mixed and ice phase clouds. Additionally, we cannot account for the ways in which smoke might have affected sample phase. For example, ice nuclei presence might facilitate the conversion of an otherwise liquid phase cloud into a mixed phase cloud that was excluded in this assessment. Alternatively, we could have included liquid clouds in our assessment that might otherwise have been present as mixed or ice phase clouds if not for the inhibition of freezing by soluble smoke compounds via the Raoult effect (discussed in Tao et al., 2012).

Aged primary smoke aerosols from ARCTAS have been found to be coated with coagulated secondary OA derived primarily from smoke (Kondo et al., 2011). These organic coatings may affect smoke CCN or IN properties (e.g., Riemer et al., 2004; Oshima et al., 2009; Kuwata et al., 2009). Interestingly, previous studies have indicated that Arctic smoke aerosols also sometimes contain an additional organic component likely to be derived from smaller, non-biomass burning particles such as sulphates and marine particles (Earle et al., 2011; Zelenyuk et al., 2010). We have presented evidence to suggest that the numerous small background particles frequently present in clean air masses in the Arctic can coagulate onto smoke-derived particles. These ultrafine particles are thought to activate at relatively low supersaturations (Lawler et al., 2014; Lohmann and Leck, 2005), and thus may have some effect on smoke aerosol properties such as hygroscopicity. The importance of this process is not well understood, but any changes in the effectiveness of smoke CCN and IN might have no-

ACPD
15, 22823–22887, 2015

ticeable impacts on Arctic clouds. Thus, the condensation of external particles onto biomass burning aerosols merits further study.

Appendix A: Description of the Kendall robust line-fit method

The Kendall robust line-fit model (also commonly known as the Theil-Sen method) (Sen, 1968; Theil, 1950) derives a linear model of a dataset from the median of the slopes between each two points in the dataset. While this method is not as commonly used as linear regressions, it performs similarly when data are normally distributed. In cases when the data are not normally distributed, this method is more appropriate than a linear regression because it reduces the impact of outliers.

Appendix B: Calculations for maximum potential contribution of background aerosol to smoke aerosol volume on 1 July 2008

The degree to which aerosol properties can be affected by the collection of Arctic background Aitken particles onto larger smoke and pollution particles depends in part on the background Aitken mode (< 80 nm diameter) particle size ranges and concentrations. These can be quite variable, as shown during several ARCTAS events from 12 April, 10 July, and 13 July 2008 (Fig. B1). Based on these spectra and associated background aerosol concentrations, we estimate that the volume of background Aitken mode aerosol ranged from 0.002–0.121 μm^3 per cm^{-3} of air during these events. As mentioned in the text, high quality size spectra for particles with diameters < 523 nm were unavailable for the 1 July 2008 smoke and background aerosol events shown in Fig. 11. Therefore, to estimate the spectra we combined the observed ranges of background air Aitken mode size spectra from other dates with the concentrations of background particles in the air mass shown in Fig. 11 ($\sim$ 2500 particles cm^{-3}) to estimate background aerosol volume. In this case, Aitken mode background aerosol volume is estimated be between 0.046–0.211 μm^3 per cm^{-3} of air.

ACPD
15, 22823–22887, 2015

To estimate full size spectra for the smoke aerosols, we combined the known size ranges of particles with diameters > 523 nm with average same-day smoke size distributions of smoke particles < 523 nm from the boundary layer. The boundary layer was the only location with full size spectra data (blue line in Fig. B1b), and while it does appear to have different size spectra for particles with >523 nm diameter, quality flagged UHSAS data from the 3–5 km haze layer (not used in this calculation) suggest that the peak at 100–200 nm diameter is similar. Based on this estimated smoke size spectra and the concentrations of smoky haze particles from Fig. 11 (~ 900 particles cm^{-3}), haze layer smoke aerosol volume for the event measured in Fig. 11 was estimated at $\sim 5.232\ \mu m^3$ per cm^{-3} of air.

Acknowledgements. The authors would like to thank A. Aknan, B. Anderson, E. Apel, G. Chen, M. Couture, T. Garrett, K. B. Huebert, A. Khain, A. Korolev, T. Lathem, P. Lawson, R. Leaitch, J. Limbacher, J. Nelson, M. Pinsky, W. Ridgeway, A. Rangno, S. Williams, S. Woods, and Y. Yang for data and/or advice or help with various aspects of this project, and all others who were involved in collecting and funding the collection of the datasets we have used. We acknowledge the Atmospheric Radiation Measurement (ARM) Program sponsored by the U.S. Department of Energy, Office of Science, Office of Biological and Environmental Research, Climate and Environmental Sciences Division for providing the ISDAC dataset. The authors also gratefully acknowledge the NOAA Air Resources Laboratory (ARL) for the provision of the HYSPLIT transport and dispersion model and/or READY website (http://www.ready.noaa.gov) used in this publication. Plots were made with Ocean Data View (Schlitzer, R., Ocean Data View, http://odv.awi.de, 2015) and R (R Core Team, 2013). CH_3CN measurements were supported by the Austrian Federal Ministry for Transport, Innovation and Technology (bmvit) through the Austrian Space Applications Programme (ASAP) of the Austrian Research Promotion Agency (FFG). T. Mikoviny is acknowledged for his support with the CH_3CN data acquisition and analysis. L. M. Zamora's funding for this study was provided by an appointment to the NASA Postdoctoral Program at Goddard Space Flight Center, administered by Oak Ridge Associated Universities through a contract with NASA. M. J. Cubison and J. L. Jimenez were supported by NASA NNX12AC03G and NNX15AH33A.

ACPD
15, 22823–22887, 2015

References

Ackerman, A. S., Toon, O. B., Stevens, D. E., Heymsfield, A. J., Ramanathan, V., and Welton, E. J.: Reduction of Tropical Cloudiness by Soot, Science, 288, 1042–1047, doi:10.1126/science.288.5468.1042, 2000.

Ackerman, A. S., Kirkpatrick, M. P., Stevens, D. E., and Toon, O. B.: The impact of humidity above stratiform clouds on indirect aerosol climate forcing, Nature, 432, 1014–1017, doi:10.1038/nature03174, 2004.

Albrecht, B. A.: Aerosols, Cloud Microphysics, and Fractional Cloudiness, Science, 245, 1227–1230, doi:10.1126/science.245.4923.1227, 1989.

Allan, J. D., Williams, P. I., Najera, J., Whitehead, J. D., Flynn, M. J., Taylor, J. W., Liu, D., Darbyshire, E., Carpenter, L. J., Chance, R., Andrews, S. J., Hackenberg, S. C., and McFiggans, G.: Iodine observed in new particle formation events in the Arctic atmosphere during ACCACIA, Atmos. Chem. Phys., 15, 5599–5609, doi:10.5194/acp-15-5599-2015, 2015.

Alvarado, M. J., Logan, J. A., Mao, J., Apel, E., Riemer, D., Blake, D., Cohen, R. C., Min, K.-E., Perring, A. E., Browne, E. C., Wooldridge, P. J., Diskin, G. S., Sachse, G. W., Fuelberg, H., Sessions, W. R., Harrigan, D. L., Huey, G., Liao, J., Case-Hanks, A., Jimenez, J. L., Cubison, M. J., Vay, S. A., Weinheimer, A. J., Knapp, D. J., Montzka, D. D., Flocke, F. M., Pollack, I. B., Wennberg, P. O., Kurten, A., Crounse, J., Clair, J. M. St., Wisthaler, A., Mikoviny, T., Yantosca, R. M., Carouge, C. C., and Le Sager, P.: Nitrogen oxides and PAN in plumes from boreal fires during ARCTAS-B and their impact on ozone: an integrated analysis of aircraft and satellite observations, Atmos. Chem. Phys., 10, 9739–9760, doi:10.5194/acp-10-9739-2010, 2010.

Avramov, A., Ackerman, A. S., Fridlind, A. M., van Diedenhoven, B., Botta, G., Aydin, K., Verlinde, J., Korolev, A. V., Strapp, J. W., McFarquhar, G. M., Jackson, R., Brooks, S. D., Glen, A., and Wolde, M.: Toward ice formation closure in Arctic mixed-phase boundary layer clouds during ISDAC, J. Geophys. Res.-Atmos., 116, D00T08, doi:10.1029/2011JD015910, 2011.

Balshi, M. S., Mcguire, A. D., Duffy, P., Flannigan, M., Kicklighter, D. W., and Melillo, J.: Vulnerability of carbon storage in North American boreal forests to wildfires during the 21st century, Glob. Change Biol., 15, 1491–1510, doi:10.1111/j.1365-2486.2009.01877.x, 2009.

Baum, B. A., Menzel, W. P., Frey, R. A., Tobin, D. C., Holz, R. E., Ackerman, S. A., Heidinger, A. K., and Yang, P.: MODIS Cloud-Top Property Refinements for Collection 6, J. Appl. Meteorol. Climatol., 51, 1145–1163, doi:10.1175/JAMC-D-11-0203.1, 2012.

ACPD
15, 22823–22887, 2015

Baumgardner, D., Jonsson, H., Dawson, W., O'Connor, D., and Newton, R.: The cloud, aerosol and precipitation spectrometer: a new instrument for cloud investigations, Atmos. Res., 59–60, 251–264, doi:10.1016/S0169-8095(01)00119-3, 2001.

Bélanger, S., Babin, M., and Tremblay, J.-É.: Increasing cloudiness in Arctic damps the increase in phytoplankton primary production due to sea ice receding, Biogeosciences, 10, 4087–4101, doi:10.5194/bg-10-4087-2013, 2013.

Bian, H., Colarco, P. R., Chin, M., Chen, G., Rodriguez, J. M., Liang, Q., Blake, D., Chu, D. A., da Silva, A., Darmenov, A. S., Diskin, G., Fuelberg, H. E., Huey, G., Kondo, Y., Nielsen, J. E., Pan, X., and Wisthaler, A.: Source attributions of pollution to the Western Arctic during the NASA ARCTAS field campaign, Atmos. Chem. Phys., 13, 4707–4721, doi:10.5194/acp-13-4707-2013, 2013.

Bourgeois, Q. and Bey, I.: Pollution transport efficiency toward the Arctic: Sensitivity to aerosol scavenging and source regions, J. Geophys. Res.-Atmos., 116, D08213, doi:10.1029/2010JD015096, 2011.

Bretherton, C. S., Blossey, P. N., and Uchida, J.: Cloud droplet sedimentation, entrainment efficiency, and subtropical stratocumulus albedo, Geophys. Res. Lett., 34, L03813, doi:10.1029/2006GL027648, 2007.

Brock, C. A., Cozic, J., Bahreini, R., Froyd, K. D., Middlebrook, A. M., McComiskey, A., Brioude, J., Cooper, O. R., Stohl, A., Aikin, K. C., de Gouw, J. A., Fahey, D. W., Ferrare, R. A., Gao, R.-S., Gore, W., Holloway, J. S., Hübler, G., Jefferson, A., Lack, D. A., Lance, S., Moore, R. H., Murphy, D. M., Nenes, A., Novelli, P. C., Nowak, J. B., Ogren, J. A., Peischl, J., Pierce, R. B., Pilewskie, P., Quinn, P. K., Ryerson, T. B., Schmidt, K. S., Schwarz, J. P., Sodemann, H., Spackman, J. R., Stark, H., Thomson, D. S., Thornberry, T., Veres, P., Watts, L. A., Warneke, C., and Wollny, A. G.: Characteristics, sources, and transport of aerosols measured in spring 2008 during the aerosol, radiation, and cloud processes affecting Arctic Climate (ARCPAC) Project, Atmos. Chem. Phys., 11, 2423–2453, doi:10.5194/acp-11-2423-2011, 2011.

Cai, Y., Montague, D. C., Mooiweer-Bryan, W., and Deshler, T.: Performance characteristics of the ultra high sensitivity aerosol spectrometer for particles between 55 and 800 nm: Laboratory and field studies, J. Aerosol Sci., 39, 759–769, doi:10.1016/j.jaerosci.2008.04.007, 2008.

Chen, Y.-C., Christensen, M. W., Xue, L., Sorooshian, A., Stephens, G. L., Rasmussen, R. M., and Seinfeld, J. H.: Occurrence of lower cloud albedo in ship tracks, Atmos. Chem. Phys., 12, 8223–8235, doi:10.5194/acp-12-8223-2012, 2012.

ACPD
15, 22823–22887, 2015

Colman, J. J., Swanson, A. L., Meinardi, S., Sive, B. C., Blake, D. R., and Rowland, F. S.: Description of the Analysis of a Wide Range of Volatile Organic Compounds in Whole Air Samples Collected during PEM-Tropics A and B, Anal. Chem., 73, 3723–3731, doi:10.1021/ac010027g, 2001.

Corr, C. A., Hall, S. R., Ullmann, K., Anderson, B. E., Beyersdorf, A. J., Thornhill, K. L., Cubison, M. J., Jimenez, J. L., Wisthaler, A., and Dibb, J. E.: Spectral absorption of biomass burning aerosol determined from retrieved single scattering albedo during ARCTAS, Atmos. Chem. Phys., 12, 10505–10518, doi:10.5194/acp-12-10505-2012, 2012.

Costantino, L. and Bréon, F.-M.: Analysis of aerosol-cloud interaction from multi-sensor satellite observations, Geophys. Res. Lett., 37, L11801, doi:10.1029/2009GL041828, 2010.

Cubison, M. J., Ortega, A. M., Hayes, P. L., Farmer, D. K., Day, D., Lechner, M. J., Brune, W. H., Apel, E., Diskin, G. S., Fisher, J. A., Fuelberg, H. E., Hecobian, A., Knapp, D. J., Mikoviny, T., Riemer, D., Sachse, G. W., Sessions, W., Weber, R. J., Weinheimer, A. J., Wisthaler, A., and Jimenez, J. L.: Effects of aging on organic aerosol from open biomass burning smoke in aircraft and laboratory studies, Atmos. Chem. Phys., 11, 12049–12064, doi:10.5194/acp-11-12049-2011, 2011.

Curry, J. A., Hobbs, P. V., King, M. D., Randall, D. A., Minnis, P., Isaac, G. A., Pinto, J. O., Uttal, T., Bucholtz, A., Cripe, D. G., Gerber, H., Fairall, C. W., Garrett, T. J., Hudson, J., Intrieri, J. M., Jakob, C., Jensen, T., Lawson, P., Marcotte, D., Nguyen, L., Pilewskie, P., Rangno, A., Rogers, D. C., Strawbridge, K. B., Valero, F. P. J., Williams, A. G., and Wylie, D.: FIRE Arctic Clouds Experiment, B. Am. Meteorol. Soc., 81, 5–29, doi:10.1175/1520-0477(2000)081<0005:FACE>2.3.CO;2, 2000.

DeCarlo, P. F., Dunlea, E. J., Kimmel, J. R., Aiken, A. C., Sueper, D., Crounse, J., Wennberg, P. O., Emmons, L., Shinozuka, Y., Clarke, A., Zhou, J., Tomlinson, J., Collins, D. R., Knapp, D., Weinheimer, A. J., Montzka, D. D., Campos, T., and Jimenez, J. L.: Fast airborne aerosol size and chemistry measurements above Mexico City and Central Mexico during the MILAGRO campaign, Atmos. Chem. Phys., 8, 4027–4048, doi:10.5194/acp-8-4027-2008, 2008.

De Gouw, J. A., Warneke, C., Parrish, D. D., Holloway, J. S., Trainer, M., and Fehsenfeld, F. C.: Emission sources and ocean uptake of acetonitrile (CH_3CN) in the atmosphere, J. Geophys. Res.-Atmos., 108, 4329, doi:10.1029/2002JD002897, 2003.

Duong, H. T., Sorooshian, A., and Feingold, G.: Investigating potential biases in observed and modeled metrics of aerosol–cloud–precipitation interactions, Atmos. Chem. Phys., 11, 4027–4037, doi:10.5194/acp-11-4027-2011, 2011.

ACPD
15, 22823–22887, 2015

Earle, M. E., Liu, P. S. K., Strapp, J. W., Zelenyuk, A., Imre, D., McFarquhar, G. M., Shantz, N. C., and Leaitch, W. R.: Factors influencing the microphysics and radiative properties of liquid-dominated Arctic clouds: Insight from observations of aerosol and clouds during ISDAC, J. Geophys. Res., 116, D00T09, doi:10.1029/2011JD015887, 2011.

Feingold, G., Remer, L. A., Ramaprasad, J., and Kaufman, Y. J.: Analysis of smoke impact on clouds in Brazilian biomass burning regions: An extension of Twomey's approach, J. Geophys. Res.-Atmos., 106, 22907–22922, doi:10.1029/2001JD000732, 2001.

Feingold, G., Eberhard, W. L., Veron, D. E., and Previdi, M.: First measurements of the Twomey indirect effect using ground-based remote sensors, Geophys. Res. Lett., 30, 1287, doi:10.1029/2002GL016633, 2003.

Fisher, J. A., Jacob, D. J., Purdy, M. T., Kopacz, M., Le Sager, P., Carouge, C., Holmes, C. D., Yantosca, R. M., Batchelor, R. L., Strong, K., Diskin, G. S., Fuelberg, H. E., Holloway, J. S., Hyer, E. J., McMillan, W. W., Warner, J., Streets, D. G., Zhang, Q., Wang, Y., and Wu, S.: Source attribution and interannual variability of Arctic pollution in spring constrained by aircraft (ARCTAS, ARCPAC) and satellite (AIRS) observations of carbon monoxide, Atmos. Chem. Phys., 10, 977–996, doi:10.5194/acp-10-977-2010, 2010.

Flannigan, M. D., Krawchuk, M. A., de Groot, W. J., Wotton, B. M., and Gowman, L. M.: Implications of changing climate for global wildland fire, Int. J. Wildland Fire, 18, 483–507, 2009.

Fridlind, A. M., van Diedenhoven, B., Ackerman, A. S., Avramov, A., Mrowiec, A., Morrison, H., Zuidema, P., and Shupe, M. D.: A FIRE-ACE/SHEBA Case Study of Mixed-Phase Arctic Boundary Layer Clouds: Entrainment Rate Limitations on Rapid Primary Ice Nucleation Processes, J. Atmos. Sci., 69, 365–389, doi:10.1175/JAS-D-11-052.1, 2012.

Fuelberg, H. E., Harrigan, D. L., and Sessions, W.: A meteorological overview of the ARCTAS 2008 mission, Atmos. Chem. Phys., 10, 817–842, doi:10.5194/acp-10-817-2010, 2010.

Garrett, T. J. and Hobbs, P. V.: Calibration of liquid water probes from the University of Washington's CV-580 aircraft at the Canadian NRC wind tunnel, in Rep. Cloud and Aerosol Research Group, 20 pp., Dep. of Atmos. Sci, Univ. of Washington, Seattle, USA, 1999.

Garrett, T. J., Zhao, C., Dong, X., Mace, G. G., and Hobbs, P. V.: Effects of varying aerosol regimes on low-level Arctic stratus, Geophys. Res. Lett., 31, L17105, doi:10.1029/2004GL019928, 2004.

Hansen, J. E. and Travis, L. D.: Light scattering in planetary atmospheres, Space Sci. Rev., 16, 527–610, doi:10.1007/BF00168069, 1974.

ACPD
15, 22823–22887, 2015

Hecobian, A., Liu, Z., Hennigan, C. J., Huey, L. G., Jimenez, J. L., Cubison, M. J., Vay, S., Diskin, G. S., Sachse, G. W., Wisthaler, A., Mikoviny, T., Weinheimer, A. J., Liao, J., Knapp, D. J., Wennberg, P. O., Kürten, A., Crounse, J. D., Clair, J. St., Wang, Y., and Weber, R. J.: Comparison of chemical characteristics of 495 biomass burning plumes intercepted by the NASA DC-8 aircraft during the ARCTAS/CARB-2008 field campaign, Atmos. Chem. Phys., 11, 13325–13337, doi:10.5194/acp-11-13325-2011, 2011.

Hegg, D. A., Nielsen, K., Covert, D. S., Jonsson, H. H., and Durkee, P. A.: Factors influencing the mesoscale variations in marine stratocumulus albedo, Tellus B, 59, 66–76, doi:10.3402/tellusb.v59i1.16970, 2007.

Hegg, D. A., Warren, S. G., Grenfell, T. C., Doherty, S. J., Larson, T. V., and Clarke, A. D.: Source Attribution of Black Carbon in Arctic Snow, Environ. Sci. Technol., 43, 4016–4021, doi:10.1021/es803623f, 2009.

Hegg, D. A., Warren, S. G., Grenfell, T. C., Doherty, S. J., and Clarke, A. D.: Sources of light-absorbing aerosol in arctic snow and their seasonal variation, Atmos. Chem. Phys., 10, 10923–10938, doi:10.5194/acp-10-10923-2010, 2010.

Heintzenberg, J., Leck, C., Birmili, W., Wehner, B., Tjernström, M., and Wiedensohler, A.: Aerosol number–size distributions during clear and fog periods in the summer high Arctic: 1991, 1996 and 2001, Tellus B, 58, 41–50, doi:10.1111/j.1600-0889.2005.00171.x, 2006.

Howell, S. G., Clarke, A. D., Freitag, S., McNaughton, C. S., Kapustin, V., Brekovskikh, V., Jimenez, J.-L., and Cubison, M. J.: An airborne assessment of atmospheric particulate emissions from the processing of Athabasca oil sands, Atmos. Chem. Phys., 14, 5073–5087, doi:10.5194/acp-14-5073-2014, 2014.

Huffman, J., Jayne, J., Drewnick, F., Aiken, A., Onasch, T., Worsnop, D., and Jimenez, J.: Design, Modeling, Optimization, and Experimental Tests of a Particle Beam Width Probe for the Aerodyne Aerosol Mass Spectrometer, Aerosol Sci. Technol., 39, 1143–1163, doi:10.1080/02786820500423782, 2005.

Intrieri, J. M., Shupe, M. D., Uttal, T., and McCarty, B. J.: An annual cycle of Arctic cloud characteristics observed by radar and lidar at SHEBA, J. Geophys. Res.-Oceans, 107, SHE 5-1–5-15, doi:10.1029/2000JC000423, 2002.

Jackson, R. C., McFarquhar, G. M., Korolev, A. V., Earle, M. E., Liu, P. S. K., Lawson, R. P., Brooks, S., Wolde, M., Laskin, A., and Freer, M.: The dependence of ice microphysics on aerosol concentration in arctic mixed-phase stratus clouds during ISDAC and M-PACE, J. Geophys. Res., 117, D15207, doi:10.1029/2012JD017668, 2012.

ACPD
15, 22823–22887, 2015

Jacob, D. J., Crawford, J. H., Maring, H., Clarke, A. D., Dibb, J. E., Emmons, L. K., Ferrare, R. A., Hostetler, C. A., Russell, P. B., Singh, H. B., Thompson, A. M., Shaw, G. E., McCauley, E., Pederson, J. R., and Fisher, J. A.: The Arctic Research of the Composition of the Troposphere from Aircraft and Satellites (ARCTAS) mission: design, execution, and first results, Atmos. Chem. Phys., 10, 5191–5212, doi:10.5194/acp-10-5191-2010, 2010.

Jouan, C., Girard, E., Pelon, J., Gultepe, I., Delanoë, J., and Blanchet, J.-P.: Characterization of Arctic ice cloud properties observed during ISDAC, J. Geophys. Res.-Atmos., 117, D23207, doi:10.1029/2012JD017889, 2012.

Karl, M., Leck, C., Gross, A., and Pirjola, L.: A study of new particle formation in the marine boundary layer over the central Arctic ocean using a flexible multicomponent aerosol dynamic model, Tellus, 64B, 17158, doi:10.3402/tellusb.v64i0.17158, 2012.

Kay, J. E. and Gettelman, A.: Cloud influence on and response to seasonal Arctic sea ice loss, J. Geophys. Res., 114, D18204, doi:10.1029/2009JD011773, 2009.

Kay, J. E,'Ecuyer, T. L, Gettelman, A., Stephens, G., and O'Dell, C.: The contribution of cloud and radiation anomalies to the 2007 Arctic sea ice extent minimum, Geophys. Res. Let., 35, L08503, doi:10.1029/2008GL033451, 2008.

King, N. J., Bower, K. N., Crosier, J., and Crawford, I.: Evaluating MODIS cloud retrievals with in situ observations from VOCALS-REx, Atmos. Chem. Phys., 13, 191–209, doi:10.5194/acp-13-191-2013, 2013.

Kondo, Y., Matsui, H., Moteki, N., Sahu, L., Takegawa, N., Kajino, M., Zhao, Y., Cubison, M. J., Jimenez, J. L., Vay, S., Diskin, G. S., Anderson, B., Wisthaler, A., Mikoviny, T., Fuelberg, H. E., Blake, D. R., Huey, G., Weinheimer, A. J., Knapp, D. J., and Brune, W. H.: Emissions of black carbon, organic, and inorganic aerosols from biomass burning in North America and Asia in 2008, J. Geophys. Res.-Atmos., 116, D08204, doi:10.1029/2010JD015152, 2011.

Korolev, A. and Isaac, G. A.: Relative Humidity in Liquid, Mixed-Phase, and Ice Clouds, J. Atmos. Sci., 63, 2865–2880, doi:10.1175/JAS3784.1, 2006.

Korolev, A. V., Strapp, J. W., Isaac, G. A., and Nevzorov, A. N.: The Nevzorov Airborne Hot-Wire LWC–TWC Probe: Principle of Operation and Performance Characteristics, J. Atmos. Ocean. Tech., 15, 1495–1510, doi:10.1175/1520-0426(1998)015<1495:TNAHWL>2.0.CO;2, 1998.

Korolev, A. V., Isaac, G. A., Cober, S. G., Strapp, J. W., and Hallett, J.: Microphysical characterization of mixed-phase clouds, Q. J. Roy. Meteor. Soc., 129, 39–65, doi:10.1256/qj.01.204, 2003.

ACPD
15, 22823–22887, 2015

Kuwata, M., Kondo, Y., and Takegawa, N.: Critical condensed mass for activation of black carbon as cloud condensation nuclei in Tokyo, J. Geophys. Res., 114, D20202, doi:10.1029/2009JD012086, 2009.

Lance, S., Shupe, M. D., Feingold, G., Brock, C. A., Cozic, J., Holloway, J. S., Moore, R. H., Nenes, A., Schwarz, J. P., Spackman, J. R., Froyd, K. D., Murphy, D. M., Brioude, J., Cooper, O. R., Stohl, A., and Burkhart, J. F.: Cloud condensation nuclei as a modulator of ice processes in Arctic mixed-phase clouds, Atmos. Chem. Phys., 11, 8003–8015, doi:10.5194/acp-11-8003-2011, 2011.

Lathem, T. L., Beyersdorf, A. J., Thornhill, K. L., Winstead, E. L., Cubison, M. J., Hecobian, A., Jimenez, J. L., Weber, R. J., Anderson, B. E., and Nenes, A.: Analysis of CCN activity of Arctic aerosol and Canadian biomass burning during summer 2008, Atmos. Chem. Phys., 13, 2735–2756, doi:10.5194/acp-13-2735-2013, 2013.

Lawler, M. J., Whitehead, J., O'Dowd, C., Monahan, C., McFiggans, G., and Smith, J. N.: Composition of 15–85 nm particles in marine air, Atmos. Chem. Phys., 14, 11557–11569, doi:10.5194/acp-14-11557-2014, 2014.

Lawson, R. P., Baker, B. A., Schmitt, C. G., and Jensen, T. L.: An overview of microphysical properties of Arctic clouds observed in May and July 1998 during FIRE ACE, J. Geophys. Res.-Atmos., 106, 14989–15014, doi:10.1029/2000JD900789, 2001.

Lebsock, M. D., Stephens, G. L., and Kummerow, C.: Multisensor satellite observations of aerosol effects on warm clouds, J. Geophys. Res.-Atmos., 113, D15205, doi:10.1029/2008JD009876, 2008.

Leck, C. and Bigg, E. K.: Aerosol production over remote marine areas – A new route, Geophys. Res. Lett., 26, 3577–3580, doi:10.1029/1999GL010807, 1999.

Leck, C. and Bigg, E. K.: Biogenic particles in the surface microlayer and overlaying atmosphere in the central Arctic Ocean during summer, Tellus B, 57, 305–316, doi:10.1111/j.1600-0889.2005.00148.x, 2005.

Lihavainen, H., Kerminen, V.-M., and Remer, L. A.: Aerosol-cloud interaction determined by both in situ and satellite data over a northern high-latitude site, Atmos. Chem. Phys., 10, 10987–10995, doi:10.5194/acp-10-10987-2010, 2010.

Lindsey, D. T. and Fromm, M.: Evidence of the cloud lifetime effect from wildfire-induced thunderstorms, Geophys. Res. Lett., 35, L22809, doi:10.1029/2008GL035680, 2008.

Lohmann, U. and Leck, C.: Importance of submicron surface-active organic aerosols for pristine Arctic clouds, Tellus B, 57, 261–268, doi:10.3402/tellusb.v57i3.16534, 2005.

ACPD
15, 22823–22887, 2015

Lubin, D. and Vogelmann, A. M.: A climatologically significant aerosol longwave indirect effect in the Arctic, Nature, 439, 453–456, doi:10.1038/nature04449, 2006.
Matsui, H., Kondo, Y., Moteki, N., Takegawa, N., Sahu, L. K., Zhao, Y., Fuelberg, H. E., Sessions, W. R., Diskin, G., Blake, D. R., Wisthaler, A., and Koike, M.: Seasonal variation of the transport of black carbon aerosol from the Asian continent to the Arctic during the ARCTAS aircraft campaign, J. Geophys. Res.-Atmos., 116, D05202, doi:10.1029/2010JD015067, 2011.
McComiskey, A. and Feingold, G.: Quantifying error in the radiative forcing of the first aerosol indirect effect, Geophys. Res. Lett., 35, L02810, doi:10.1029/2007GL032667, 2008.
McComiskey, A. and Feingold, G.: The scale problem in quantifying aerosol indirect effects, Atmos. Chem. Phys., 12, 1031–1049, doi:10.5194/acp-12-1031-2012, 2012.
McComiskey, A., Feingold, G., Frisch, A. S., Turner, D. D., Miller, M. A., Chiu, J. C., Min, Q., and Ogren, J. A.: An assessment of aerosol-cloud interactions in marine stratus clouds based on surface remote sensing, J. Geophys. Res.-Atmos., 114, D09203, doi:10.1029/2008JD011006, 2009.
McConnell, J. R., Edwards, R., Kok, G. L., Flanner, M. G., Zender, C. S., Saltzman, E. S., Banta, J. R., Pasteris, D. R., Carter, M. M., and Kahl, J. D. W.: 20th-Century Industrial Black Carbon Emissions Altered Arctic Climate Forcing, Science, 317, 1381–1384, doi:10.1126/science.1144856, 2007.
McFarquhar, G. M., Zhang, G., Poellot, M. R., Kok, G. L., McCoy, R., Tooman, T., Fridlind, A., and Heymsfield, A. J.: Ice properties of single-layer stratocumulus during the Mixed-Phase Arctic Cloud Experiment: 1. Observations, J. Geophys. Res.-Atmos., 112, D24201, doi:10.1029/2007JD008633, 2007.
McFarquhar, G. M., Ghan, S., Verlinde, J., Korolev, A., Strapp, J. W., Schmid, B., Tomlinson, J. M., Wolde, M., Brooks, S. D., Cziczo, D., Dubey, M. K., Fan, J., Flynn, C., Gultepe, I., Hubbe, J., Gilles, M. K., Laskin, A., Lawson, P., Leaitch, W. R., Liu, P., Liu, X., Lubin, D., Mazzoleni, C., Macdonald, A.-M., Moffet, R. C., Morrison, H., Ovchinnikov, M., Shupe, M. D., Turner, D. D., Xie, S., Zelenyuk, A., Bae, K., Freer, M., and Glen, A.: Indirect and semi-direct aerosol campaign: The Impact of Arctic Aerosols on Clouds, B. Am. Meteorol. Soc., 92, 183–201, 2011.
McNaughton, C. S., Clarke, A. D., Freitag, S., Kapustin, V. N., Kondo, Y., Moteki, N., Sahu, L., Takegawa, N., Schwarz, J. P., Spackman, J. R., Watts, L., Diskin, G., Podolske, J., Holloway, J. S., Wisthaler, A., Mikoviny, T., de Gouw, J., Warneke, C., Jimenez, J., Cubison, M., Howell,

ACPD
15, 22823–22887, 2015

S. G., Middlebrook, A., Bahreini, R., Anderson, B. E., Winstead, E., Thornhill, K. L., Lack, D., Cozic, J., and Brock, C. A.: Absorbing aerosol in the troposphere of the Western Arctic during the 2008 ARCTAS/ARCPAC airborne field campaigns, Atmos. Chem. Phys., 11, 7561–7582, doi:10.5194/acp-11-7561-2011, 2011.

Moore, R. H., Bahreini, R., Brock, C. A., Froyd, K. D., Cozic, J., Holloway, J. S., Middlebrook, A. M., Murphy, D. M., and Nenes, A.: Hygroscopicity and composition of Alaskan Arctic CCN during April 2008, Atmos. Chem. Phys., 11, 11807–11825, doi:10.5194/acp-11-11807-2011, 2011.

Moore, R. H., Karydis, V. A., Capps, S. L., Lathem, T. L., and Nenes, A.: Droplet number uncertainties associated with CCN: an assessment using observations and a global model adjoint, Atmos. Chem. Phys., 13, 4235–4251, doi:10.5194/acp-13-4235-2013, 2013.

Morales, R. and Nenes, A.: Characteristic updrafts for computing distribution-averaged cloud droplet number and stratocumulus cloud properties, J. Geophys. Res.-Atmos., 115, D18220, doi:10.1029/2009JD013233, 2010.

Morales, R., Nenes, A., Jonsson, H., Flagan, R. C., and Seinfeld, J. H.: Evaluation of an entraining droplet activation parameterization using in situ cloud data, J. Geophys. Res.-Atmos., 116, D15205, doi:10.1029/2010JD015324, 2011.

Morrison, H., de Boer, G., Feingold, G., Harrington, J., Shupe, M. D., and Sulia, K.: Resilience of persistent Arctic mixed-phase clouds, Nat. Geosci., 5, 11–17, doi:10.1038/ngeo1332, 2012.

Orellana, M. V., Matrai, P. A., Leck, C., Rauschenberg, C. D., Lee, A. M., and Coz, E.: Marine microgels as a source of cloud condensation nuclei in the high Arctic, P. Natl. Acad. Sci., 108, 13612–13617, doi:10.1073/pnas.1102457108, 2011.

Oshima, N., Koike, M., Zhang, Y., and Kondo, Y.: Aging of black carbon in outflow from anthropogenic sources using a mixing state resolved model: 2. Aerosol optical properties and cloud condensation nuclei activities, J. Geophys. Res., 114, D18202, doi:10.1029/2008JD011681, 2009.

Peng, Y., Lohmann, U., Leaitch, R., Banic, C., and Couture, M.: The cloud albedo-cloud droplet effective radius relationship for clean and polluted clouds from RACE and FIRE.ACE, J. Geophys. Res.-Atmos., 107, AAC 1-1–AAC 1-6, doi:10.1029/2000JD000281, 2002.

Platnick, S., King, M. D., Ackerman, S. A., Menzel, W. P., Baum, B. A., Riedi, J. C., and Frey, R. A.: The MODIS cloud products: algorithms and examples from Terra, IEEE Trans. Geosci. Remote Sens., 41, 459–473, doi:10.1109/TGRS.2002.808301, 2003.

ACPD
15, 22823–22887, 2015

Quinn, P. K., Bates, T. S., Miller, T. L., Coffman, D. J., Johnson, J. E., Harris, J. M., Ogren, J. A., Forbes, G., Anderson, T. L., Covert, D. S., and Rood, M. J.: Surface submicron aerosol chemical composition: What fraction is not sulfate?, J. Geophys. Res.-Atmos., 105, 6785–6805, doi:10.1029/1999JD901034, 2000.

Quinn, P. K., Miller, T. L., Bates, T. S., Ogren, J. A., Andrews, E., and Shaw, G. E.: A 3-year record of simultaneously measured aerosol chemical and optical properties at Barrow, Alaska, J. Geophys. Res., 107, 4130, doi:10.1029/2001JD001248, 2002.

R Core Team.: R: A language and environment for statistical computing, R Foundation for Statistical Computing, Vienna, Austria, available at: http://www.R-project.org/ (last access: 5 August 2015), 2013.

Raatikainen, T., Moore, R. H., Lathem, T. L., and Nenes, A.: A coupled observation – modeling approach for studying activation kinetics from measurements of CCN activity, Atmos. Chem. Phys., 12, 4227–4243, doi:10.5194/acp-12-4227-2012, 2012.

Rangno, A. L. and Hobbs, P. V.: Ice particles in stratiform clouds in the Arctic and possible mechanisms for the production of high ice concentrations, J. Geophys. Res.-Atmos., 106, 15065–15075, doi:10.1029/2000JD900286, 2001.

Riemer, N., Vogel, H., and Vogel, B.: Soot aging time scales in polluted regions during day and night, Atmos. Chem. Phys., 4, 1885–1893, doi:10.5194/acp-4-1885-2004, 2004.

Rosenfeld, D., Fromm, M., Trentmann, J., Luderer, G., Andreae, M. O., and Servranckx, R.: The Chisholm firestorm: observed microstructure, precipitation and lightning activity of a pyro-cumulonimbus, Atmos. Chem. Phys., 7, 645–659, doi:10.5194/acp-7-645-2007, 2007.

Rosenfeld, D., Wang, H., and Rasch, P. J.: The roles of cloud drop effective radius and LWP in determining rain properties in marine stratocumulus, Geophys. Res. Lett., 39, L13801, doi:10.1029/2012GL052028, 2012.

Rosenfeld, D., Fischman, B., Zheng, Y., Goren, T., and Giguzin, D.: Combined satellite and radar retrievals of drop concentration and CCN at convective cloud base, Geophys. Res. Lett., 41, 3259–3265, doi:10.1002/2014GL059453, 2014.

Sachse, G. W., Hill, G. F., Wade, L. O., and Perry, M. G.: Fast response, high precision carbon monoxide sensor using a tunable diode laser absorption technique, J. Geophys. Res., 92, 2071–2081, 1987.

Sen, P. K.: Estimates of the Regression Coefficient Based on Kendall's Tau, J. Am. Stat. Assoc., 63, 1379–1389, doi:10.1080/01621459.1968.10480934, 1968.

ACPD
15, 22823–22887, 2015

Shantz, N. C., Gultepe, I., Liu, P. S. K., Earle, M. E., and Zelenyuk, A.: Spatial and temporal variability of aerosol particles in Arctic spring, Q. J. Roy. Meteor. Soc., 138, 2229–2240, doi:10.1002/qj.1940, 2012.

Shantz, N. C., Gultepe, I., Andrews, E., Zelenyuk, A., Earle, M. E., Macdonald, A. M., Liu, P. S. K., and Leaitch, W. R.: Optical, physical, and chemical properties of springtime aerosol over Barrow Alaska in 2008, Int. J. Climatol., 34, 3125–3138, doi:10.1002/joc.3898, 2014.

Shao, H. and Liu, G.: Influence of mixing on evaluation of the aerosol first indirect effect, Geophys. Res. Lett., 33, L14809, doi:10.1029/2006GL026021, 2006.

Shaw, G. E.: The Arctic Haze Phenomenon, B. Am. Meteorol. Soc., 76, 2403–2413, doi:10.1175/1520-0477(1995)076<2403:TAHP>2.0.CO;2, 1995.

Shinozuka, Y. and Redemann, J.: Horizontal variability of aerosol optical depth observed during the ARCTAS airborne experiment, Atmos. Chem. Phys., 11, 8489–8495, doi:10.5194/acp-11-8489-2011, 2011.

Singh, H. B., Anderson, B. E., Brune, W. H., Cai, C., Cohen, R. C., Crawford, J. H., Cubison, M. J., Czech, E. P., Emmons, L., Fuelberg, H. E., Huey, G., Jacob, D. J., Jimenez, J. L., Kaduwela, A., Kondo, Y., Mao, J., Olson, J. R., Sachse, G. W., Vay, S. A., Weinheimer, A., Wennberg, P. O., and Wisthaler, A.: Pollution influences on atmospheric composition and chemistry at high northern latitudes: Boreal and California forest fire emissions, Atmos. Environ., 44, 4553–4564, doi:10.1016/j.atmosenv.2010.08.026, 2010.

Soja, A. J., Stocks, B., Maczek, P., Fromm, M., Servranckx, R., and Turetsky, M.: ARCTAS: the perfect smoke, Can. Smoke Newsl., International Association of Wildland Fire, Missoula, MT, USA, 2–7, 2008.

Stephens, G. L.: Radiation Profiles in Extended Water Clouds. I: Theory, J. Atmospheric Sci., 35, 2111–2122, doi:10.1175/1520-0469(1978)035<2111:RPIEWC>2.0.CO;2, 1978.

Stocks, B. J., Fosberg, M. A., Lynham, T. J., Mearns, L., Wotton, B. M., Yang, Q., Jin, J.-Z., Lawrence, K., Hartley, G. R., Mason, J. A., and McKENNEY, D. W.: Climate Change and Forest Fire Potential in Russian and Canadian Boreal Forests, Climatic Change, 38, 1–13, doi:10.1023/A:1005306001055, 1998.

Stohl, A., Andrews, E., Burkhart, J. F., Forster, C., Herber, A., Hoch, S. W., Kowal, D., Lunder, C., Mefford, T., Ogren, J. A., Sharma, S., Spichtinger, N., Stebel, K., Stone, R., Ström, J., Tørseth, K., Wehrli, C., and Yttri, K. E.: Pan-Arctic enhancements of light absorbing aerosol concentrations due to North American boreal forest fires during summer 2004, J. Geophys. Res., 111, D22214, doi:10.1029/2006JD007216, 2006.

ACPD
15, 22823–22887, 2015

Stohl, A., Berg, T., Burkhart, J. F., Fjæraa, A. M., Forster, C., Herber, A., Hov, Ø., Lunder, C., McMillan, W. W., Oltmans, S., Shiobara, M., Simpson, D., Solberg, S., Stebel, K., Ström, J., Tørseth, K., Treffeisen, R., Virkkunen, K., and Yttri, K. E.: Arctic smoke – record high air pollution levels in the European Arctic due to agricultural fires in Eastern Europe in spring 2006, Atmos. Chem. Phys., 7, 511–534, doi:10.5194/acp-7-511-2007, 2007.

Stone, R. S.: Variations in western Arctic temperatures in response to cloud radiative and synoptic-scale influences, J. Geophys. Res.-Atmos., 102, 21769–21776, doi:10.1029/97JD01840, 1997.

Strapp, J. W., Leaitch, W. R., and Liu, P. S. K.: Hydrated and Dried Aerosol-Size-Distribution Measurements from the Particle Measuring Systems FSSP-300 Probe and the Deiced PCASP-100X Probe, J. Atmos. Ocean. Tech., 9, 548–555, doi:10.1175/1520-0426(1992)009<0548:HADASD>2.0.CO;2, 1992.

Tao, W.-K., Chen, J.-P., Li, Z., Wang, C., and Zhang, C.: Impact of aerosols on convective clouds and precipitation, Rev. Geophys., 50, RG2001, doi:10.1029/2011RG000369, 2012.

Theil, H.: A rank-invariant method of linear and polynomial regression analysis, Proc. R. Neth. Acad. Sci. LIII,1397–1412, 1950.

Tietze, K., Riedi, J., Stohl, A., and Garrett, T. J.: Space-based evaluation of interactions between aerosols and low-level Arctic clouds during the Spring and Summer of 2008, Atmos. Chem. Phys., 11, 3359–3373, doi:10.5194/acp-11-3359-2011, 2011.

Twomey, S.: The Influence of Pollution on the Shortwave Albedo of Clouds, J. Atmospheric Sci., 34, 1149–1152, doi:10.1175/1520-0469(1977)034<1149:TIOPOT>2.0.CO;2, 1977.

Vavrus, S., Holland, M. M., and Bailey, D. A.: Changes in Arctic clouds during intervals of rapid sea ice loss, Clim. Dynam., 36, 1475–1489, doi:10.1007/s00382-010-0816-0, 2010.

Warneke, C., Bahreini, R., Brioude, J., Brock, C. A., Gouw, J. A. de, Fahey, D. W., Froyd, K. D., Holloway, J. S., Middlebrook, A., Miller, L., Montzka, S., Murphy, D. M., Peischl, J., Ryerson, T. B., Schwarz, J. P., Spackman, J. R., and Veres, P.: Biomass burning in Siberia and Kazakhstan as an important source for haze over the Alaskan Arctic in April 2008, Geophys. Res. Lett., 36, L02813, doi:10.1029/2008GL036194, 2009.

Warneke, C., Froyd, K. D., Brioude, J., Bahreini, R., Brock, C. A., Cozic, J., de Gouw, J. A., Fahey, D. W., Ferrare, R., Holloway, J. S., Middlebrook, A. M., Miller, L., Montzka, S., Schwarz, J. P., Sodemann, H., Spackman, J. R., and Stohl, A.: An important contribution to springtime Arctic aerosol from biomass burning in Russia, Geophys. Res. Lett., 37, L01801, doi:10.1029/2009GL041816, 2010.

ACPD
15, 22823–22887, 2015

Wisthaler, A., Hansel, A., Dickerson, R. R., and Crutzen, P. J.: Organic trace gas measurements by PTR-MS during INDOEX 1999, J. Geophys. Res.-Atmos., 107, 8024, doi:10.1029/2001JD000576, 2002.

Zelenyuk, A., Yang, J., Choi, E., and Imre, D.: SPLAT II: An Aircraft Compatible, Ultra-Sensitive, High Precision Instrument for In-Situ Characterization of the Size and Composition of Fine and Ultrafine Particles, Aerosol Sci. Technol., 43, 411–424, doi:10.1080/02786820802709243, 2009.

Zelenyuk, A., Imre, D., Earle, M., Easter, R., Korolev, A., Leaitch, R., Liu, P., Macdonald, A. M., Ovchinnikov, M., and Strapp, W.: In Situ Characterization of Cloud Condensation Nuclei, Interstitial, and Background Particles Using the Single Particle Mass Spectrometer, SPLAT II†, Anal. Chem., 82, 7943–7951, doi:10.1021/ac1013892, 2010.

Zelenyuk, A., Imre, D., Wilson, J., Zhang, Z., Wang, J., and Mueller, K.: Airborne single particle mass spectrometers (SPLAT II & miniSPLAT) and new software for data visualization and analysis in a geo-spatial context, J. Am. Soc. Mass Spectrom., 26, 257–270, doi:10.1007/s13361-014-1043-4, 2015.

Zhao, C. and Garrett, T. J.: Effects of Arctic haze on surface cloud radiative forcing, Geophys. Res. Lett., 42, 557–564, doi:10.1002/2014GL062015, 2015.

Zhao, C., Klein, S. A., Xie, S., Liu, X., Boyle, J. S., and Zhang, Y.: Aerosol first indirect effects on non-precipitating low-level liquid cloud properties as simulated by CAM5 at ARM sites, Geophys. Res. Lett., 39, L08806, doi:10.1029/2012GL051213, 2012.

Zuidema, P., Baker, B., Han, Y., Intrieri, J., Key, J., Lawson, P., Matrosov, S., Shupe, M., Stone, R., and Uttal, T.: An Arctic Springtime Mixed-Phase Cloudy Boundary Layer Observed during SHEBA, J. Atmos. Sci., 62, 160–176, doi:10.1175/JAS-3368.1, 2005.

ACPD
15, 22823–22887, 2015

Table 1. Instrumentation used in this study from the ARCTAS dataset. Data were collected at 1 s resolution, unless noted otherwise.

	ARCTAS-A 1–19 April; -CARB 29 June; -B 1–13 July, 2008		
	Instrument	Range	Uncertainty
N_{liq}, r_e, and LWC	Cloud, Aerosol and Precipitation Spectrometer – Cloud and Aerosol Spectrometer (CAPS-CAS)	0.5–50 µm	unknown (not validated with another dataset)
phase	none (see text)	liquid only	NA
CN	TSI Condensation Particle Counter (CPC) 3010	> 0.01 µm	precision 5 %
	TSI CPC 3025	> 0.003 µm	precision 10 %
	TSI Aerodynamic Particle Sizer (APS) 3321	0.583–7.75 µm	NA
	DMT Ultra High Sensitivity Aerosol Spectrometer (UHSAS)	0.0609–0.986 µm	~ 5 %, but increases in air with > 3000 particles cm^{-3} (Cai et al., 2008)
Temperature	Rosemount 102 E4AL	−65 to +35 °C	±1 °C
Relative humidity	Aircraft-Integrated Meteorological Measurement System (AIMMS-20)	–	2 %
hline CCN	DMT continuous-flow, streamwise thermal-gradient CCN counter	–	7–16 % (Moore et al., 2011)
CO	Tunable Diode Laser Absorption Spectrometer (TDLAS)	–	±2 % (Sachse et al., 1987)
Submicron sulfate[a]	Time-of-Flight Aerosol Mass Spectrometer	–	±35 % (DeCarlo et al., 2008)
Submicron OA[a]	Time-of-Flight Aerosol Mass Spectrometer	–	38 % (Huffman et al., 2005)
BC mass[a]	Single-Particle Soot Photometer (SP2)	–	±10 % (Moteki and Kondo, 2008)
CH_3CN	Proton Transfer Reaction – Mass Spectrometer (PTR-MS)	–	±10 % (Wisthaler et al., 2002)
CH_2Cl_2[b]	Electron Capture Detection and Mass Spectrometer	–	±10 % or ±2 pptv (Colman et al., 2001)
Total backscatter (550 nm)[a]	TSI 3563 Integrating Nephelometer	> 0.1 $M m^{-1}$	0.5 $M m^{-1}$

[a] Data were collected at 10 s resolution.
[b] Data were collected at ~ 40 s resolution.

ACPD
15, 22823–22887, 2015

Table 2. Instrumentation used in this study from the ISDAC dataset. Data were collected at 1 s resolution.

	ISDAC, 1–29 April, 2008		
	Instrument	Range	Uncertainty
N_{liq}, r_e, LWC	DMT Cloud Droplet Probe (CDP)	2–50 µm	~20 % (Earle et al., 2011)
N_{liq}*	Forward Scattering Spectrometer Probe (FSSP) model 100	0.3–47 µm	~17 % (Baumgardner, 1983)
LWC*, r_e	FSSP-100	0.3–47 µm	~34 % (Baumgardner, 1983)
phase	Cloud Particle Imager (CPI)	40 µm–2 mm	NA
CN	PMS airborne Passive Cavity Aerosol Spectrometer Probe (PCASP)-100X	~0.12–3 µm	7 % (Earle et al., 2011)
	TSI CPC 3775	> 0.004 µm (Shantz et al., 2014)	±10 % (Shantz et al., 2014)
Temperature	Rosemont 102 probe	−65 to +35 °C	±1 °C
Relative humidity	EG7G chilled-mirror hygrometer	–	–
CCN	DMT continuous-flow, streamwise thermal-gradient CCN counter (reported between 14–37 % supersaturation)	–	7–16 % (Moore et al., 2011)
Total dry backscatter (550 nm)	TSI 3563 Integrating Nephelometer	> 0.1 M m^{-1}	±0.5 M m^{-1}

* For days when high quality CDP data were unavailable, following Earle et al. (2011).

ACPD
15, 22823–22887, 2015

Table 3. Instrumentation used in this study from the NRC FIRE.ACE dataset. Data were collected at 1 s resolution.

	NRC FIRE.ACE, 1–29 April, 1998		
	Instrument	Range	Uncertainty
N_{liq}	FSSP-100	0.3–47 µm	~ 17 % (Baumgardner, 1983)
LWC, r_e	FSSP-100	0.3–47	up to 25 % (Peng et al., 2002)
LWC	King probe	0.05–3 g m^{-3}	±10 % or larger (Peng et al., 2002)
	Nevzorov probe	~ 0.006–1 g m^{-3}	±15 % (Korolev et al., 1998)
phase	CPI	40 µm–2 mm	NA
Temperature	Rosemont probe	−65 to +35 °C	±1 °C in-cloud, ±2–3 °C out-of-cloud
Relative humidity	LiCor Hygrometer	0–90 %	NA
CN	PCASP 100X	0.12–3 µm	7 % (Earle et al., 2011)
CCN	Cloud condensation nucleus counter (reported at 57–72 % supersaturation)	n/a	±10 %

ACPD
15, 22823–22887, 2015

Table 4. Instrumentation used in this study from the UW FIRE.ACE dataset. Data were collected at 1 s resolution.

	UW FIRE.ACE, 19 May–24 June, 1998		
	Instrument	Range	Uncertainty
N_{liq}	FSSP-100	0.3–47 µm	~ 17 % (Baumgardner, 1983)
LWC, r_e	FSSP-100	0.3–47 µm	see Table 5
LWC	Gerber Scientific PVM-100X	0.01–0.75 g m^{-3}	12 % (Garrett and Hobbs, 1999)
phase	CPI	40 µm–2 mm	not available
CN	PCASP 100X	0.12–3 µm	7 % (Earle et al., 2011)
Temperature	Rosemount Model 102CY2CG and 414L bridge	−60 to +40 °C	< 0.1 °C
Relative humidity	In-House Scanning Humidigraph	30–80 %	not available
Total dry backscatter (550 nm)	MS Electron Integrating Nephelometer	>0.1 M m^{-1}	not available

ACPD
15, 22823–22887, 2015

Table 5. Comparison of LWC measurements ($g\,m^{-3}$) from various instruments

Campaign	LWC determination method	slope	y-intercept	R^2 value
UW FIRE.ACE	FSSP vs. Gerber Scientific PVM-100X[a] (Gerber et al., 1994)	0.84	−0.009	0.91
NRC FIRE.ACE[b]	FSSP-96 vs. King probe (King et al., 1978)	0.79	0.007	0.94
	FSSP-96 vs. Nevzorov probe (Korolev et al., 1998)	0.84	0.017	0.84
	Nevzorov vs. King	0.84	0.002	0.89

[a] For Gerber LWC < 0.5 $g\,m^{-3}$. Above that, the FSSP missed known rain/drizzle events with larger droplets, and that began to impact the linear relationship.
[b] Samples with clearly problematic data (e.g., LWC < 0 $g\,m^{-3}$, or highly inconsistent values when all other measurements were consistent) were given a quality flag and discarded.

ACPD
15, 22823–22887, 2015

Table 6. A comparison of background concentrations of biomass burning and pollution tracers as previously reported to those in the ARCTAS dataset in air masses that would be defined as background using only the CN_{PCASP} equivalent[a] cutoff of ≤ 127 particles cm^{-3}.

Tracer (units)	Median (interquartile range)	95th percentile	Previously reported background concentrations
CO (ppbv)	96 (92–108)	157	150–170[c–g]
CH_3CN (ppbv)	0.08 (0.065–0.110)	0.21	0.1[g,h]
BC ($\mu g\,C\,m^{-3}$)	0.001 (0.001–0.003)	0.014	0.029[e]
Submicron SO_4^{2-} ($\mu g\,m^{-3}$)[b]	0.031 (0.01–0.08)	0.34	0.5–0.9[e,h,i]

[a] CN_{PCASP} values were not available in ARCTAS, and were thus approximated from the CN concentrations from the APS and UHSAS for the same size range as would be measured in the PCASP.
[b] Following Fisher et al., 2011, we assume ARCTAS submicron sea-salt SO_4^{2-} is negligible, and that total submicron SO_4^{2-} is approximately equal to submicron non seasalt-SO_4^{2-}.
[c] Stohl et al. (2007).
[d,e] Warneke et al. (2009, 2010).
[f] Brock et al. (2011).
[g] Moore et al. (2011).
[h] Lathem et al. (2013).
[i,j] Quinn et al. (2000, 2002).

ACPD
15, 22823–22887, 2015

Table 7. Median properties and ranges for all background and biomass burning cloud cases in the multi-campaign assessment.

Property	Background (n = 19)	Biomass burning (n = 6)
Aerosol number concentration (CN^{*}_{PCASP}), cm^{-3}	42 (1–767)	1986 (422–18169)
CCN, cm^{-3}	31 (6–332)	1394 (68–6670)
Backscatter at 550 nm, Mm^{-1}	0.7 (−0.19–1.13)	6.5 (0.3–44.1)
Temperature, °C	−5 (−20–7)	4 (0–10)
Pressure, mbar	848 (505–995)	757 (687–840)
Liquid water content (LWC), $g\,m^{-3}$	0.09 (0.01–0.66)	0.06 (0.02–0.74)
Cloud droplet effective radius (r_e), µm	8.1 (5.0–12.7)	3.5 (2.3–8.6)
Droplet number concentration (N_{liq}), cm^{-3}	38 (12–464)	321 (182–377)

* CN_{PCASP} equivalent data.

ACPD
15, 22823–22887, 2015

Table 8. Median properties and ranges for the 1 July 2008 ARCTAS case study, including background, intermediate, and biomass burning cloud cases.

Property	Background (n = 3)	Intermediate (n = 3)	Biomass burning (n = 2)
Aerosol number concentration (CN^{*}_{PCASP}), cm^{-3}	329 (107–452)	308 (147–427)	2604 (2207–3001)
CCN, cm^{-3}	545 (205–592)	795 (462–908)	10879 (10348–11411)
Backscatter at 550 nm, Mm^{-1}	2.1 (0.9–3.0)	3.3 (1.6–4.7)	35.7 (31.2–40.2)
Temperature, °C	0.8 (0.2–0.9)	0.1 (−0.1–3.1)	2.8 (2.4–3.1)
Pressure, mbar	770 (762–792)	768 (763–826)	808
Liquid water content (LWC), $g\,m^{-3}$	0.03 (0.01–0.12)	0.02 (0.01–0.04)	0.02 (0.01–0.02)
Cloud droplet effective radius (r_e), µm	5.1 (4.5–7.6)	3.4 (2.9–4.5)	2.5 (2.4–2.7)
Droplet number concentration (N_{liq}), cm^{-3}	402 (332–525)	720 (621–907)	937 (825–1048)

* Or CN_{PCASP} equivalent for ARCTAS data.

ACPD
15, 22823–22887, 2015

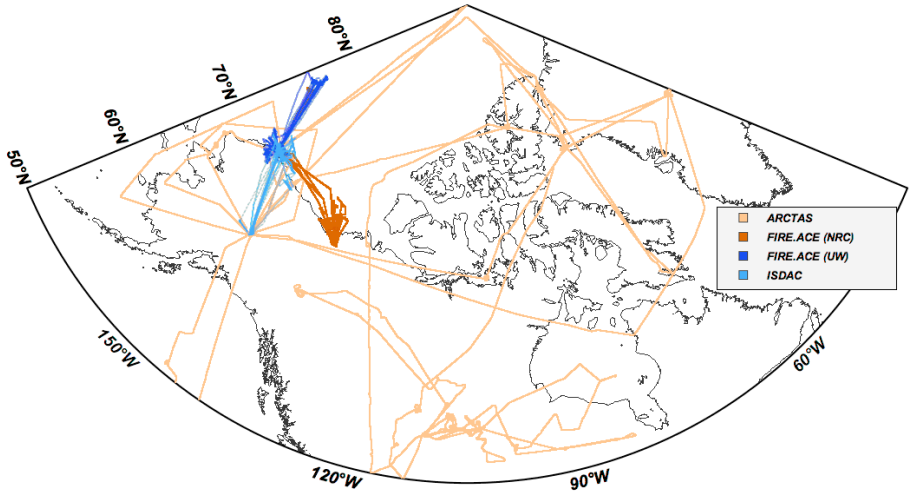

Figure 1. Sampling locations for the following campaigns: ARCTAS (light orange), NRC FIRE.ACE (dark orange), UW FIRE.ACE (dark blue), and ISDAC (light blue). The locations of clouds sampled are shown in Fig. 4.

ACPD
15, 22823–22887, 2015

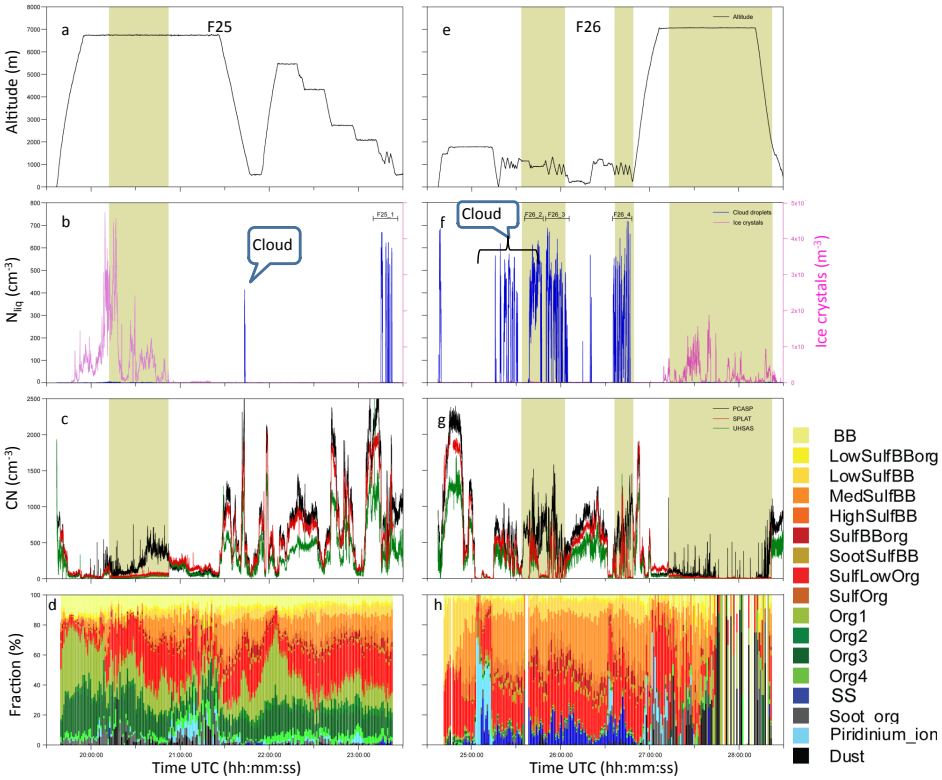

Figure 2. ISDAC 2008 aerosol and flight characteristics near and in selected clouds influenced by biomass burning from 19 April (left) and 20 April (right). Flight characteristics shown include: **(a)** altitude, **(b)** LWC (blue) and IWC (pink), **(c)** aerosol concentration from the PCASP (black), SPLAT (red), and UHSAS (green) instruments, and **(d)** bulk aerosol SPLAT chemical composition. Tan shading indicates SPLAT sampling through the in-cloud CVI inlet.

ACPD
15, 22823–22887, 2015

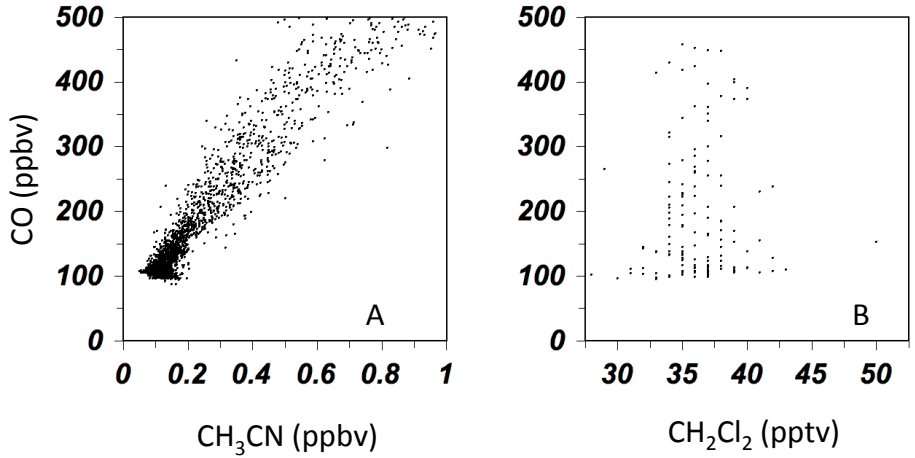

Figure 3. Carbon monoxide (ppbv) during the 1 July 2008 ARCTAS-B flight as a function of **(a)** the biomass burning tracer CH_3CN (ppbv) and **(b)** the fossil fuel combustion tracer CH_2Cl_2 (pptv).

ACPD
15, 22823–22887, 2015

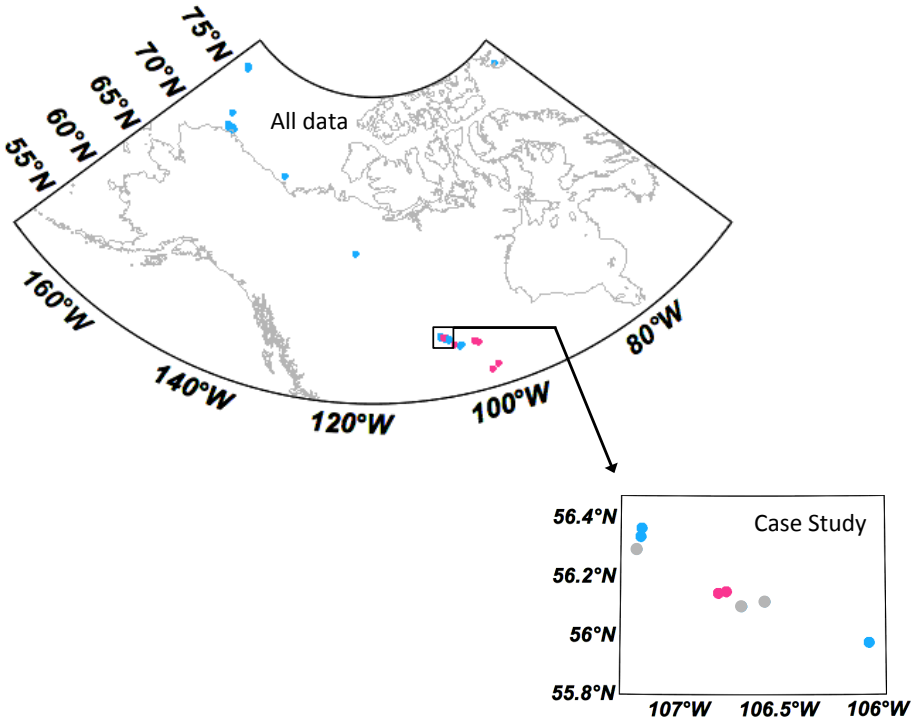

Figure 4. Map of cloud sample locations from all campaigns. Red points indicate biomass burning samples, blue cases indicate background samples, and grey points indicate intermediate samples.

ACPD
15, 22823–22887, 2015

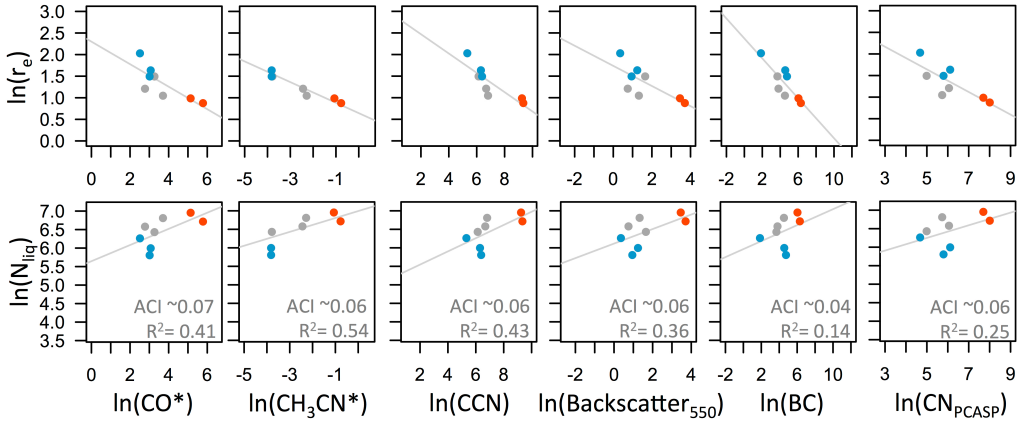

Figure 5. Based on eight samples from the ARCTAS-B 1 July 2008 case study, here we show the relationships between $\ln(r_e)$ (top row) and $\ln(N_{liq})$ (bottom row) and $\ln(BB_t)$ derived from six indicators (where BB_t = CO (ppbv) (* indicates background values of 99.2 ppbv have been subtracted), CH_3CN (ppbv) (* indicates background values of 0.088 ppbv have been subtracted), CCN (cm^{-3}), backscatter at 550 nm (Mm^{-1}), BC ($\mu g\,C\,m^{-3}$), and CN_{PCASP} equivalent values (cm^{-3}), as calculated from UHSAS and APS measurements. Biomass burning samples are noted in red, and background samples are noted in blue. To show variation between tracers, linear regressions and associated ACI estimates are shown in light gray (but note that final ACI values are not derived from individual regressions, but rather a combination of all six tracers).

ACPD
15, 22823–22887, 2015

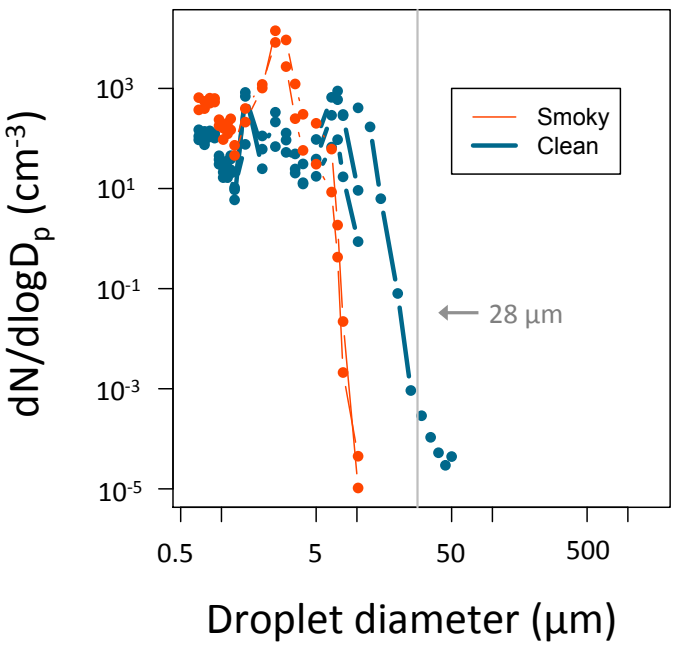

Figure 6. Cloud droplet size distributions for individual case study biomass burning clouds (thin orange lines) and clean background clouds (thick blue lines).

ACPD
15, 22823–22887, 2015

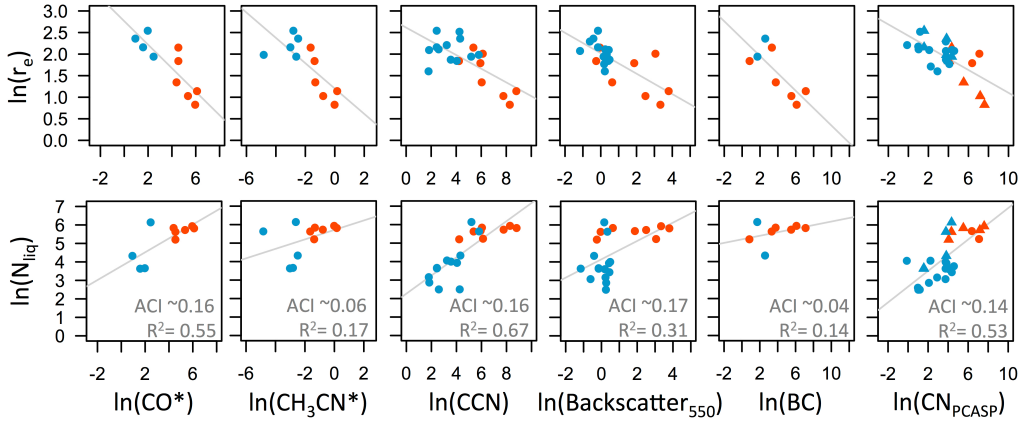

Figure 7. Same as in Fig. 5, but for data from the multi-campaign analysis. For CH_3CN, the * indicates background values of 0.018 ppbv have been subtracted (due to low background CH_3CN levels in some of the samples).

ACPD
15, 22823–22887, 2015

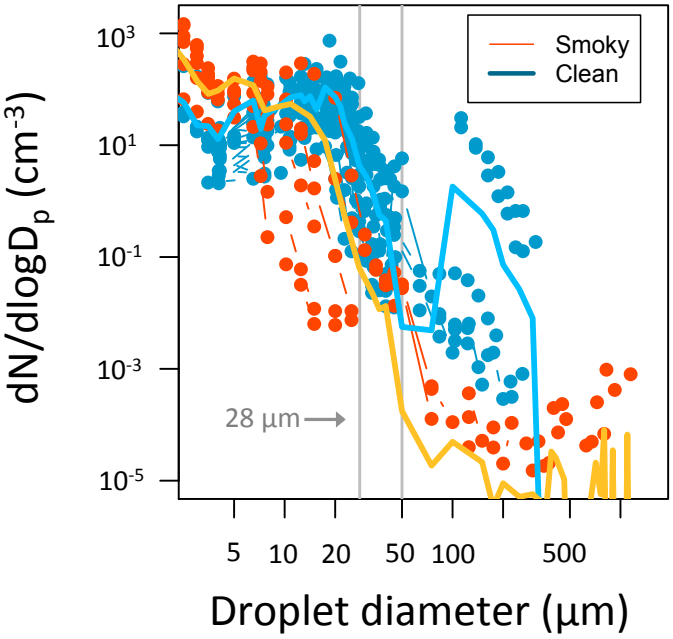

Figure 8. Mean cloud particle size distributions (µm) for all non-case study biomass burning clouds (orange) and clean background clouds (blue). The 28 and 50 µm lines are marked in grey. Light orange and blue lines indicate mean values for binned size classes for smoky and clean clouds, respectively, including zero values not shown on the log-log plot.

ACPD
15, 22823–22887, 2015

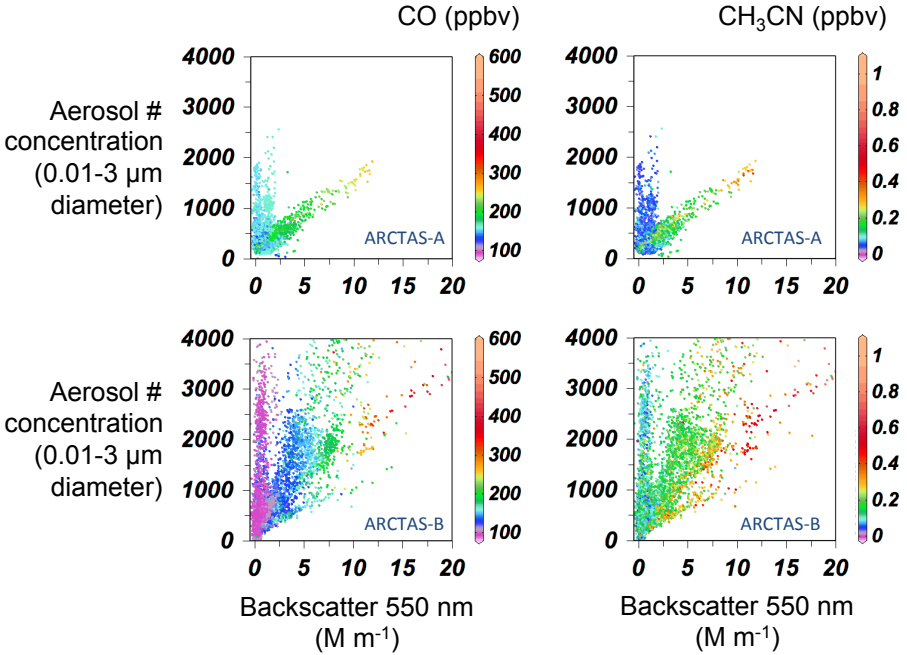

Figure 9. Relationships between ARCTAS aerosol number concentration, backscatter, the combustion tracer CO, and the biomass burning tracer CH_3CN at altitudes < 5.2 km in spring ARCTAS-A (top) and summer ARCTAS-B (bottom) out-of-cloud air masses. To show detail in the ARCTAS-B panels, some high values are not shown.

ACPD
15, 22823–22887, 2015

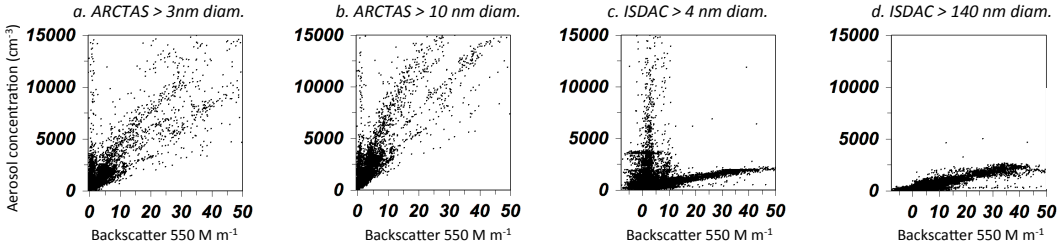

Figure 10. The relationship between out-of-cloud aerosol concentration and backscatter at 550 nm given different lower-end particle size cutoffs in the **(a, b)** ARCTAS and **(c, d)** ISDAC datasets. Ultrafine aerosols appear to dominate the high aerosol number concentration/low backscatter particles seen in panels **(a–c)**, as shown by their disappearance when a diameter cutoff of 140 nm is used **(d)**. Measurements are from the following instruments: **(a)** TSI 3025, **(b)** TSI 3010, **(c)** TSI 3775, and **(d)** PCASP. To show detail, some high values along both axes are not shown.

ACPD
15, 22823–22887, 2015

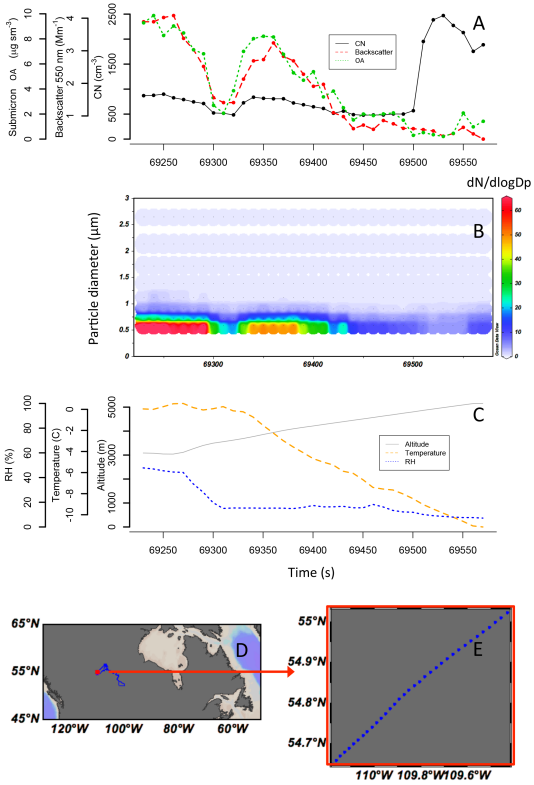

Figure 11. Relationships between **(a)** bulk CN_{TSI}, backscatter, and submicron OA concentrations, **(b)** APS aerosol concentrations in bins from 0.58–3.0 µm, **(c)** and altitude, temperature and relative humidity along the ARCTAS-B flight track from 1 July 2008 (shown in panel **d**), for data within the area boxed in red (shown in higher resolution in panel **e**) as the airplane moved north. Data are shown as a function of seconds UTC since the start of the date on which measurements began.

ACPD
15, 22823–22887, 2015

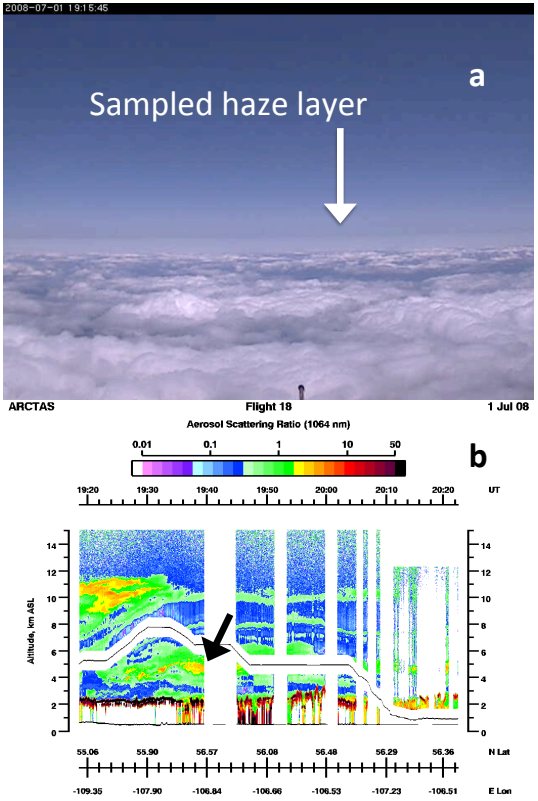

Figure 12. Images of the haze layer sampled at ~3–5 km altitude in Fig. 11 from **(a)** on-board aircraft video and **(b)** the DIAL instrument (data from http://science.larc.nasa.gov/lidar/arctas/dial_18.html). Arrows point out the presence of the haze layer sampled in Fig. 11.

ACPD
15, 22823–22887, 2015

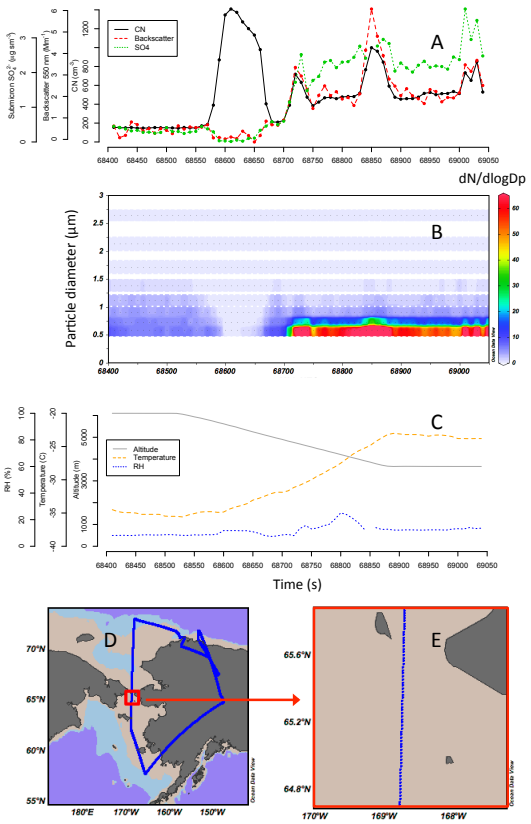

Figure 13. Relationships between **(a)** bulk CN_{TSI}, backscatter, and submicron SO_4^{2-} concentration, **(b)** APS aerosol concentrations in bins from 0.58–3.0 µm, **(c)** and altitude, temperature and relative humidity along the ARCTAS-A flight track from 12 April 2008 (shown in panel **d**), for data within the area boxed in red (shown in higher resolution in panel **e**) as the airplane moved north. Data are shown as a function of seconds UTC since the start of the date on which measurements began.

ACPD
15, 22823–22887, 2015

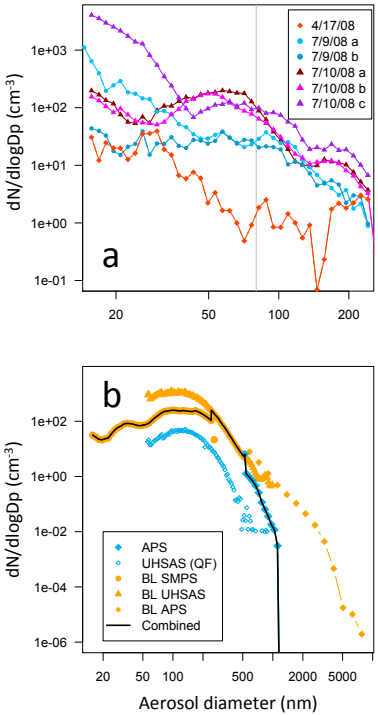

Figure B1. Mean out-of-cloud aerosol particle size distributions for **(a)** several ARCTAS background aerosol events, and **(b)** smoke cases on 1 July 2008. Some days had multiple background aerosol events; these are distinguished in panel **(a)** by color and the letters a–c. The light grey line in panel **(a)** is the 80 nm cutoff used here to distinguish Aitken mode particles from accumulation mode particles. **(b)** APS and UHSAS values (in blue) are from the 3–5 km altitude haze layer described in Fig. 11. Other data (shown in orange) are the boundary layer (BL) smoke spectra. The UHSAS data from the 3–5 km altitude haze layer had a quality flag, and were not used to determine the estimated size spectra (shown as the black line). Note that panels **(a)** and **(b)** have different axes values.

ACPD
15, 22823–22887, 2015